Journal Pre-proof

Hybrid wire - arc additive manufacture and effect of rolling process on microstructure and tensile properties of Inconel 718

Tao Zhang, Huigui Li, Hai Gong, Jialuo Ding, Yunxin Wu, Chenglei Diao, Xiaoyong Zhang, Stewart Williams

PII: S0924-0136(21)00321-6

DOI: https://doi.org/10.1016/j.jmatprotec.2021.117361

Reference: PROTEC 117361

To appear in: *Journal of Materials Processing Tech.*

Received Date: 1 June 2021

Revised Date: 28 August 2021

Accepted Date: 4 September 2021

Please cite this article as: Zhang T, Li H, Gong H, Ding J, Wu Y, Diao C, Zhang X, Williams S, Hybrid wire - arc additive manufacture and effect of rolling process on microstructure and tensile properties of Inconel 718, *Journal of Materials Processing Tech.* (2021), doi: https://doi.org/10.1016/j.jmatprotec.2021.117361

Journal of Materials Processing Technology, Volume 299, January 2022 Article number 117361
DOI:10.1016/j.jmatprotec.2021.117361

Hybrid wire - arc additive manufacture and effect of rolling process on microstructure and tensile properties of Inconel 718

Tao Zhang [a,b], Huigui Li [a,b], Hai Gong [a,b *], Jialuo Ding [c], Yunxin Wu [a,b], Chenglei Diao [c], Xiaoyong Zhang [d], Stewart Williams [c]

[a] Light Alloy Research Institute, Central South University, Changsha 410083, China

[b] State Key Laboratory of High Performance Complex Manufacturing, Central South University, Changsha 410083, China

[c] Welding Engineering and Laser Processing Centre, Cranfield University, Bedford, MK43 0AL, UK

[d] School of Materials Science and Engineering, Nanjing University of Science and Technology, Nanjing, 210094, China

*** Corresponding author**

E-mail: gonghai@csu.edu.cn (H. Gong)

Highlights:

- Rolling process is integrated into the WAAM to refine the grains.
- A new heat treatment is applied for Inconel 718 to further enhance the strengths.
- The columnar dendrites change to equiaxed grains with interlayer rolling process.
- Finer grains and isotropic mechanical properties are obtained in warm rolling.
- The strengthening mechanism of the hybrid WAAM and rolling process is revealed.

Abstract:

Wire - arc additive manufacture (WAAM) is suitable for Inconel 718 components due to its high deposition efficiency. However, large columnar dendrites decrease the mechanical properties and can cause severe mechanical anisotropy. Cold rolling and warm rolling through flame heating have been investigated to analyze their effects on microstructure and tensile properties compared to as-deposited WAAM material. Standard solution and double aging (SA), as well as homogenization followed by solution and aging (HSA) heat treatments were compared. The results show that the large columnar dendrites change to finer equiaxed grains 16.4 μm and 26.2 μm in size for warm and cold rolled alloy, respectively. This increases to 22.5 μm and 30.1 μm after HSA treatment. The microhardness and strength of rolled material increase significantly and the warm rolled material after HSA treatment exceeds that of the wrought alloy. While the as-deposited and cold rolled samples both show significant anisotropy, isotropic tensile properties are obtained for warm rolled plus HSA heat treated samples. Finer equiaxed grains with more dispersive distributions of γ' and γ'' strengthening precipitation contribute to the superior mechanical properties for warm rolled material. For both the cold and warm rolled material, there was an elongation decrease due to precipitated particles, which also led to a trans-granular ductile fracture mode. The strengthening mechanism of the hybrid rolling process was analyzed and found to be related to work hardening, grain boundary strengthening, precipitated strengthening phases and the δ phase.

Key words: Wire - arc additive manufacture; hybrid rolling process; microstructure; tensile properties; strengthening mechanism

1 Introduction

Inconel 718 (IN-718) is a precipitation strengthened alloy with the advantages of high strength, good creep resistance, weldability and fatigue performance, as discussed by Zhang et al. (2018). Baufeld (2012) reported that IN-718 is widely used in critical components of engines in aerospace, such as turbine discs and blades due to its high-temperature stability (under 650℃). IN-718 accounted for 70% of Ni-base alloys in components of GE engines and over 50% for the Trent 800 turbofan engine of Roll-Royce. IN-718 is strengthened through

precipitation of secondary phases into an austenitic matrix (γ phase). The secondary phases consist of γ" (Ni_3Nb), γ' ($Ni_3(Al, Ti)$), δ (Ni_3Nb), Laves ($(Ni, Cr, Fe)_2(Nb, Mo, Ti)$) phase and MC carbides ((Nb, Ti) (C, N)), as reported by Chen et al. (2021). The γ" and γ' phases are the main strengthening phases after heat treatment. The δ phase is the stable phase of the γ" phase at high temperatures, and the nucleation of δ phase is generated inside the γ" phase with high stacking fault. Therefore, the compositions of these two phases are the same. Watring et al. (2020) found that brittle Laves phase and MC carbides were detrimental to the mechanical properties of IN 718.

Additive Manufacturing (AM) has been widely considered as a new manufacturing process for many aerospace applications. Jafari et al. (2021) concluded that Wire - Arc Additive Manufacture (WAAM), using an electric arc as the heat source and metal wire as the feedstock, can produce medium to large components because of its high-rate deposition and potentially unlimited build size. Raut et al. (2021) reported that the wire arc additively manufactured (WAAMed) material's mechanical properties were comparable to wrought or cast material. However, there were significant challenges associated with WAAM such as undesirable microstructures and mechanical properties, high residual stresses, and distortion. Thus, more research was still needed to handle the above challenges by optimizing the process parameters and post-deposition heat treatment. Compared to powder based AM processes, such as powder bed fusion (PBF), WAAM features a high material utilization and deposition rate.

Most previous studies of AM of IN-718 focused on PBF. Tucho et al. (2017) investigated the microstructure and segregation in the as-printed and the solution heat-treated states of IN-718 in PBF. The microstructure of the as-printed parts exhibited non-columnar grains, but contained well-shaped columnar/cellular sub-grains. Deng et al. (2018) found that in PBF the IN-718 samples in building direction had a lower tensile strength but a higher ductility compared to that in the travel direction of the laser head, the mechanism was shown to be partly due to crystallographic features but more importantly due to different amounts of residual stress and dislocations

accumulated in these two kinds of samples. As IN-718 is mainly strengthened by precipitation after heat treatment, heat treatment was vital for the microstructure evolution and mechanical properties enhancement. Li et al. (2019) studied the effects of the solution and double aging treatment on the mechanical properties of IN-718 by PBF, founding that the hardness of the IN-718 superalloy first increased and then decreased with the increasing of the solution temperature. Cao et al. (2018) studied the microstructure and precipitation in PBF-made IN 718 after solution and double-aging treatment and found disc-shaped and cuboidal γ″, circular γ′ precipitates and plate-like δ phases precipitated at grain boundaries and also within the interior of austenite matrix. The morphology, distribution and crystallography of these precipitates and their formation mechanisms were analyzed and discussed. Schneider et al. (2018) evaluated the microstructure of IN-718 in PBF after various heat treatments, such as homogenization, solution and double aging process as well as its combination. This study showed that increased strength without sacrificing tensile ductility could be achieved with reduced number of heat treatment cycles.

In recent years, a few studies of WAAM IN-718 have been published. Asala et al. (2017) studied the extensive formation of eutectic solidification micro constituents during WAAM of IN-718; this included Laves and MC carbides, induced by micro-segregation produced by tungsten inert gas (TIG) process. Clark et al. (2008) adopted metal inert gas (MIG) for WAAM of IN-718 alloy, which proved to be a cost effective fabrication process. The Laves and δ phases, which were detrimental to mechanical properties, were formed through localized chemical segregation. Cold Metal Transfer (CMT) process was used for deposition of IN-718 with torch shielding using pure argon. Xu et al. (2019) concluded that oxides formed during the CMT deposition had no effect on the tensile properties of IN-718 as the 0.5 μm thick passivation layer (consisting of Cr_2O_3 and Al_2O_3) prevented further oxides from forming inside the bulk. Xu et al. (2018) studied the microstructure and mechanical properties of IN-718 deposited by WAAM using the plasma arc process. Large columnar grains developed along the building

direction, with the length and width as large as 11 mm and 0.8 mm, inferior mechanical properties and severe anisotropy were observed.

Coules et al. (2013) applied high pressure rolling process to the weld seam to reduce the residual stress. This rolling process produced a weld material with a greater yield strength and hardness, but slightly reduced impact toughness compared to unrolled welds. Rolling was also found to completely change the residual stress state in the weld, creating large compressive longitudinal residual stresses. Martina et al. (2015) integrated inter-pass cold rolling into the WAAM process for improving microstructure and material properties of WAAM deposited Ti-6Al-4V alloy. The undesirable coarse-columnar primary β grain structures (centimeter scale) generated in WAAM process can be refined down to 100 μm by applying interlayer cold rolling for Ti-6Al-4V alloy. which significantly increases the tensile strength and greatly improves material isotropy. Colegrove et al. (2017) reported that the cold rolling applied in-process during WAAM can provide significant benefits in reducing residual stresses and distortion, and giving isotropic mechanical properties that can be better than the wrought material for Ti-6Al-4V alloy. Mei et al. (2015) investigated the effect of cold rolling on the precipitation kinetics of intermediate phases in IN-718 alloy with isothermal aging at 800 °C for 8 h. The evolution of δ-phase with cold rolling is characterized using SEM at a lower magnification and the evolution of γ″-phase with cold rolling is characterized at a higher magnification. With the increase in the degree of cold rolling, the content and the size of intragranular γ″-phase decreased obviously, and the morphology of γ″-phase gradually becomes more spherical. Moreover, the cold rolling promoted γ″→δ transformation with the increase of rolling load as cold rolling reduced the time of γ″-phase reaching the saturation value and γ″→δ transformation initiating. Zhang et al. (2016) studied the coarsening behaviors of γ″ phase in IN-718 during aging process and found that the existence of the δ phase retarded the formation and coarsening of the γ″ phase, without influencing its final particle size or amount. Moreover, when a 50% reduction of cold rolling was applied, the dimensions of the γ″ particles were decreased

with increased aging time. Hu et al. (2021) proposed a novel printing technology of hybrid in situ rolled wire + arc additive manufacturing (HRAM), which was a capable of fabricating large-scale components by combining in situ micro-rolling with standard WAAM, proving to be effective in enhancing the ductility and tensile strength of the resulting parts. Xu et al. (2018) applied the interlayer cold rolling process to plasma deposited IN-718 alloy, founding that the columnar grains can be refined to small equiaxed grains. This was explained by the authors that the deformation energy provided by rolling triggers non-uniform recrystallization upon successive depositions. As a result, the mechanical strength and elongation of the 75 kN cold rolled material exceeds the wrought strength of IN-718 alloy after a standard heat treatment, conforming to Aerospace Material Specifications (AMS-5662M). However, it was found that the refined microstructure with 75 kN inter-pass cold rolling process was not uniform. The microstructure consisted of alternating bands of finely equiaxed grains and small columnar grains in between the bands. Therefore, warm rolling was considered in this study to increase the deformation depth without the need to increase the rolling force in order to further refine the grains.

In this study, interlayer warm rolling was applied through flame heating the material. The comparisons of hardness, microstructure and precipitation as well as tensile properties in warm rolled conditions are conducted with the comparisons to as-deposited and cold rolled ones. In addition, a new heat treatment was investigated to all the samples compared to the standard heat treatment for IN-718. The fracture morphology and strengthening mechanism of different rolled materials are also discussed.

2 Materials and Methods

2.1 Set up of hybrid WAAM deposition and inter-layer rolling

The experimental set up of hybrid WAAM deposition and inter-layer rolling system of IN-718 is shown in Fig.1. The WAAM deposition system consists of a CMT power source (Fronius, CMT 4000 advanced), a CMT

torch, a wire feeder (Fronius, VR 7000) and a 6-axis ABB robot. The hydraulic rolling system consists of a flat roller, a hydraulic cylinder and a CNC system to control the motion of the rolling system.

To study the effects of cold rolling and warm rolling on microstructure and tensile properties on WAAM deposited IN-718 alloy, three comparative walls were built: as-deposited, inter-layer cold rolled, and inter-layer warm rolled with flame heating. Zig-zag path was adopted in this study to decrease the height difference between both ends of the deposited walls, as shown in Fig.1. The roller started to move on the top surface of the deposited material when the temperature on the top surface of the material cools down to room temperature, this was the cold rolling process. The experimental set up of flame-heated warm rolling and the position of thermocouples is shown in Fig.2. After deposition of each layer, flame heating with oxyacetylene was applied on one side of the wall to a target temperature of 450 ℃. Then the roller started to move on the top surface of the deposited material with a temperature of 450 ℃, this was the warm rolling process. The recrystallization temperature of IN-718 was over 1000 ℃, which is much higher than the target temperature in flame heating process. Therefore, only warm rolling instead of hot rolling was investigated in this study due to the limitation of temperature increase using flame heating. Several thermocouples were attached on the other side of the wall to monitor the temperature during the flame heating process. Camera was also adopted to monitor the overall temperature distribution of the wall. The experimental parameters of the hybrid deposition and interlayer rolling process are shown in Table 1. The wire diameter of IN718 was 1.2 mm and its compositions (wt.%) were: 53.15Ni-19.42Cr-5.22Nb+Ta-2.95Mo-0.96Ti-0.47Al-0.41Cu-0.11Mn-Bal.Fe.

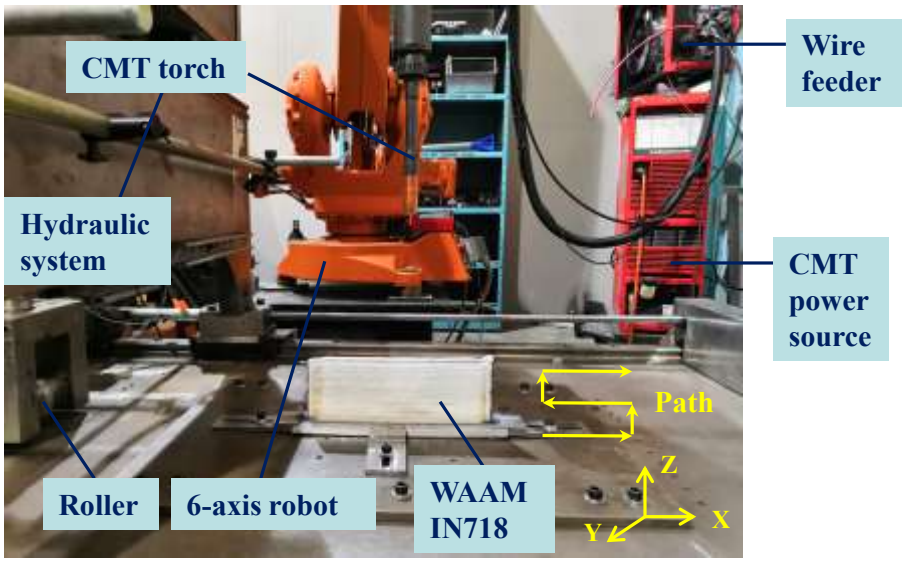

Fig.1 Experimental set up of hybrid WAAM deposition and rolling system

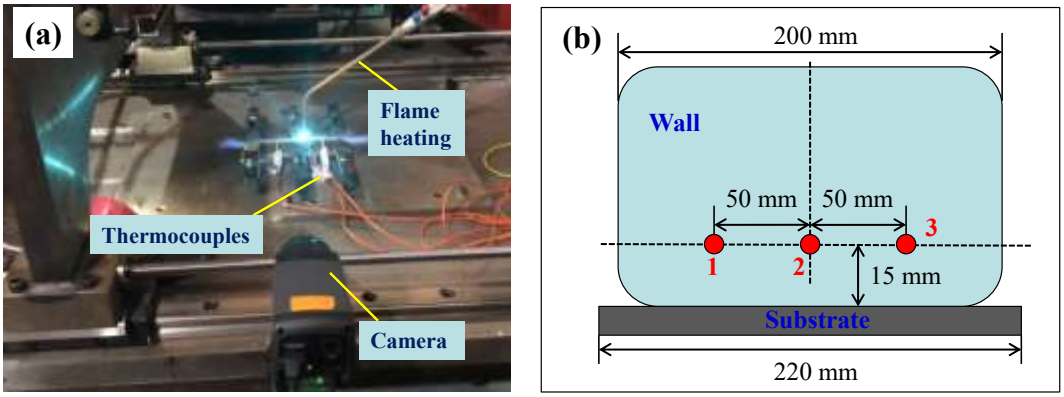

Fig.2 (a): Experimental set up of flame heating; (b) Positions of thermocouples

Table 1 Experimental parameters for hybrid deposition and rolling process

Parameter	Value
Contact tip-to-work distance	14 mm
Wire feed speed	7 m/min
Torch travel speed	6 mm/s

Rolling force	50 kN
Roller diameter	100 mm
Roller width	20 mm
Roller travel speed	5 mm/s
Inter-pass cooling time	3 mins
Shielding gas flow rate	15 L/min

2.2 Heat treatment

After deposition and the inter-layer rolling process, the standard heat treatment conforming to Aerospace Material Specifications (AMS-5662M) was applied as follows: solution treatment at 970 ℃and held for 1 h followed by water quenching; double-aging treatment at 720 ℃ and held for 8 h; furnace cooling to 620 ℃ and held for 8 h followed by air cooling. The schematic diagrams of different heat treatments are presented in Fig.3. The Laves phase generated during the WAAM process is detrimental to mechanical properties of IN-718 and it cannot be eliminated during solution and double-aging (SA) process alone, as reported by Chlebus et al. (2015). Therefore, in this study, another homogenization plus solution and double-aging (HSA) heat treatment was investigated. The homogenization procedure was that the material was heated to 1020℃ and held for 1h followed by air cooling. The solution and double-aging treatment in HSA is the same with standard SA process.

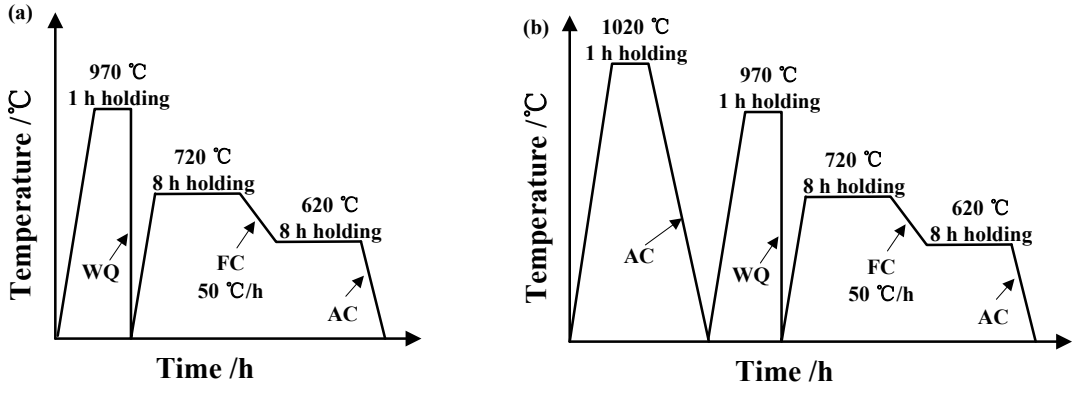

Fig.3 Schematic diagrams of different heat treatments: (a) solution and double-aging SA; (b) homogenization plus solution and double-aging (HSA). (WQ: water quenching; FC: furnace cooling; AC: air cooling)

2.3 Analysis methods

Samples after different hybrid manufacturing and heat treatment processes were cross-sectioned and further microstructure and microhardness analysis. The analysis on the microstructure and microhardness was conducted on the cross section (YZ plane), which is perpendicular to the moving direction of the torch. The microhardness test was applied across the layers from the top surface to the bottom part of the walls with an interval of 1 mm using a Zwick/Roell hardness tester under a load of 1 Kg and a holding time of 15 s. Microstructure and second precipitates were observed using an optical microscopy (OM, OPTIPHOT, NIKON) and a scanning electron microscopy (SEM, FEI XL30-SFEG). An energy dispersive spectrometry (EDS, OXFORD INSTRUMENTS) was used for element analysis. The OM samples were ground with 240, 1200 and 2500 grit SiC papers under flowing water and then polished with 3 μm diamond and 0.5 μm colloidal silica. The microstructure before heat treatment was revealed through electrolytic etching in 10% oxalic acid solution with a voltage of 6 V and an etching time of 10 s. The grain boundary of the material after heat treatment was revealed by Kalling's NO.2 etchant (5 g copper chloride, 100 ml hydrochloric acid and 100 ml ethanol).

Tensile coupons were machined along horizontal (X direction) and vertical (Z direction) direction of the IN-718 walls, as shown in Fig.1. The gauge length was 19.6 mm and its dimension was shown in Fig.4, according to BS EN 2001-1:2005 standard. Room temperature tensile tests were conducted on Instron 5500R electro-mechanical machine with a load cell of 30 kN and a crosshead speed of 1 mm/min. A laser extensometer was used to measure the variation of the gauge length during the tensile test for the calculation of the elongation. Three samples were tested for each condition and the average value as well as the error was obtained.

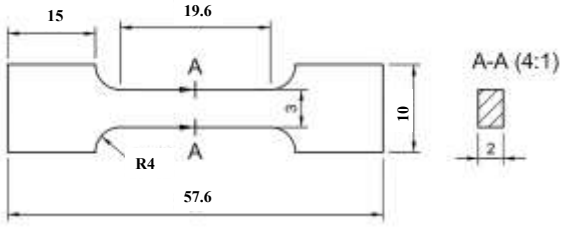

Fig.4 Dimensions of IN 718 tensile coupon (unit: mm)

3 Results and discussions

It is quite difficult to control the temperature accurately during the flame heating process for warm rolling. It took about 3 mins to reach 450~500 ℃ monitored by the thermocouples. Thermocouple 3 failed during the deposition and rolling process. The temperature variation using thermocouples is shown in Fig.5. Therefore, the roller started to move when the temperature just exceeds 450℃ for each layer. Fig.6 and Table 2 shows the size and strain of the walls under the conditions of as deposited, cold rolled and warm rolled. The length of three walls is 200 mm. The rolling process increases the width of the walls, which increases from 10.65 mm to 11.05 mm and 11.81 mm in cold and warm rolled conditions, respectively. The calculation method of deformation for each layer is shown in Eq.(1). The average layer height decreased from 2.82 mm in the as deposited (AD) condition to 2.34 mm in the warm rolled (WR) condition. Therefore, 17% strain was estimated for the WR, which is much larger than 8.5% in cold rolled (CR) condition.

$$\varepsilon = \frac{h_{\mathrm{de}} - h_{\mathrm{rolled}}}{h_{\mathrm{de}}} \times 100\% \qquad (1)$$

where h_{de} is layer height of WAAM deposition, h_{rolled} is layer height after the rolling processes.

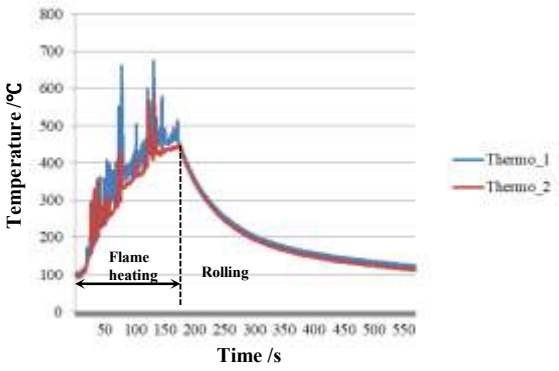

Fig.5 Temperature variation during flame heating

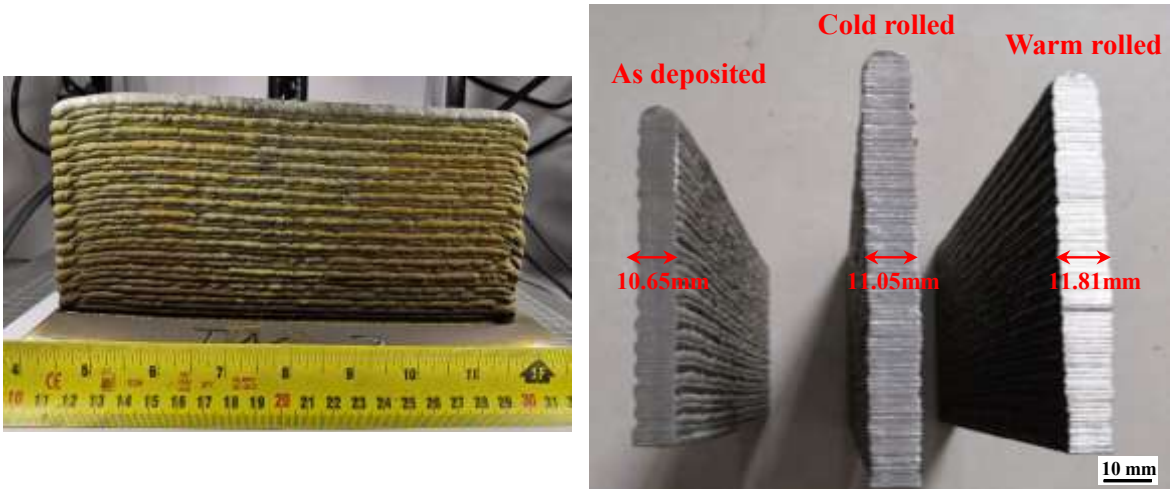

(a) Wall size

(b) Cross section of walls

Fig.6 Dimensions of three walls on different conditions: (a) wall size; (b) cross section of walls

Table 2 Size and strain of walls

	Layers	Total height (mm)	Average layer height (mm)	Strain (%)	Wall width (mm)	Rolling pressure (MPa)
AD	32	90.24	2.82	/	10.65	/
CR (50 kN)	36	93.24	2.59	8.51	11.05	1384.4
WR (50 kN)	36	84.24	2.34	17.02	11.81	958.3

AD: as deposited; CR: cold rolled; WR: warm rolled

3.1 Microhardness

Fig.7 shows the microhardness distribution of the walls in the as deposited, cold rolled and warm rolled conditions. There is a significant hardness increase of 72 HV and 58 HV for the cold rolled and warm rolled material, respectively. Meanwhile, the hardness fluctuation increases after the rolling process, and greater in the warm rolled condition than in the cold rolled condition. This may be explained in that during the warm rolling process, the inter-layer temperature could not keep perfectly consistent for each layer by using the flame heating method. It can be seen from Fig.5 that the temperature fluctuation is significant during the flame heating process and the temperature accuracy is quite difficult to be controlled using flame heating. Inconsistent temperature for each layer results in strain heterogeneity in warm rolling, thus inducing obvious microhardness fluctuation. Although larger deformation is generated during the warm rolling, the hardness after the warm rolling is slightly lower than that in the cold rolling. It is known that deformation resistance decreases with increased temperature. Thus during the warm rolling process, apart from work hardening, material softening is also taking place. This results in a lower microhardness in the warm rolled condition compared to the cold rolled material

The microhardness values of the materials under all the three conditions increase significantly after heat treatment, as shown in Table 3. After standard SA heat treatment, the microhardness values show dramatic increases of 156 HV, 107 HV and 130 HV for as deposited, cold and warm rolled walls, respectively. This is because of the precipitation process during the heat treatment which is the main strengthening mechanism of IN-718. The microhardness can be slightly further increased by HSA treatment. After both heat treatments, the microhardness in the warm rolled condition exceeds the value in the cold rolled condition. The microhardness fluctuation using HSA heat treatment is smaller than that using standard SA.

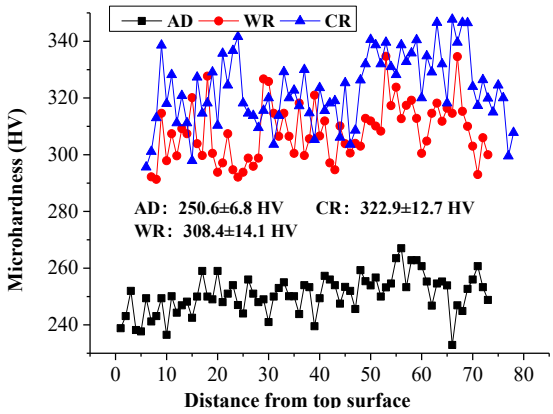

Fig.7 Microhardness distribution of walls after deposition, cold and warm rolling process

Table 3 Average microhardness after heat treatments

Heat treatment	AD	CR	WR
SA	406.8±18.6	427.1±17.8	438.2±20.7
HSA	412.7±12.2	438.1±13.3	457±17.5

SA: solution and double-aging; HSA: homogenization plus solution and double-aging

3.2 Microstructure

Fig. 8 shows the microstructure of the as deposited, warm rolled and cold rolled materials. Columnar dendrites with an average dendrite arm spacing of 83 μm are formed along the building direction (Z direction in Fig. 1), which can be several millimeters long. Many dark precipitated particles are formed at inter-dendritic boundaries, which are marked with arrows in Fig. 8(a). According to the EDS analysis, the segregated particles are Laves phase which is rich in Nb, Mo and Ti; while the matrix of IN-718 mainly consists of Ni, Cr and Fe, as shown in Fig. 9. The columnar dendrites are fragmentized and change to equiaxed grains after both the cold and warm rolling processes. After the rolling process on one deposited layer, the subsequent new layer deposition is conducted on the rolled surface, which introduces high heat input to the rolled surface. The deformation energy

induced by the rolling processes plays a positive role in triggering recrystallization through the high heat input from the following layer of WAAM deposition. The average grain size in the warm rolled material is 16.4 μm and the grains are smaller and more uniformly distributed compared to the grains in the cold rolled material (26.2 μm). Only Laves phase and MC carbides are precipitated during WAAM deposition and no strengthening phases are generated. Standard SA and HSA heat treatments are adopted to improve the mechanical properties of the material. The HSA heat treatments do not change the grain morphology of the as deposited material and columnar dendrites remain after heat treatment, as shown in Fig. 10. However, it can be seen that the amount of Laves phase is decreased during the homogenization treatment. After HSA heat treatment, there is grain growth for the rolled materials and the average grain sizes increased to 22.5 μm and 30.1 μm for the warm rolled and cold rolled material, respectively.

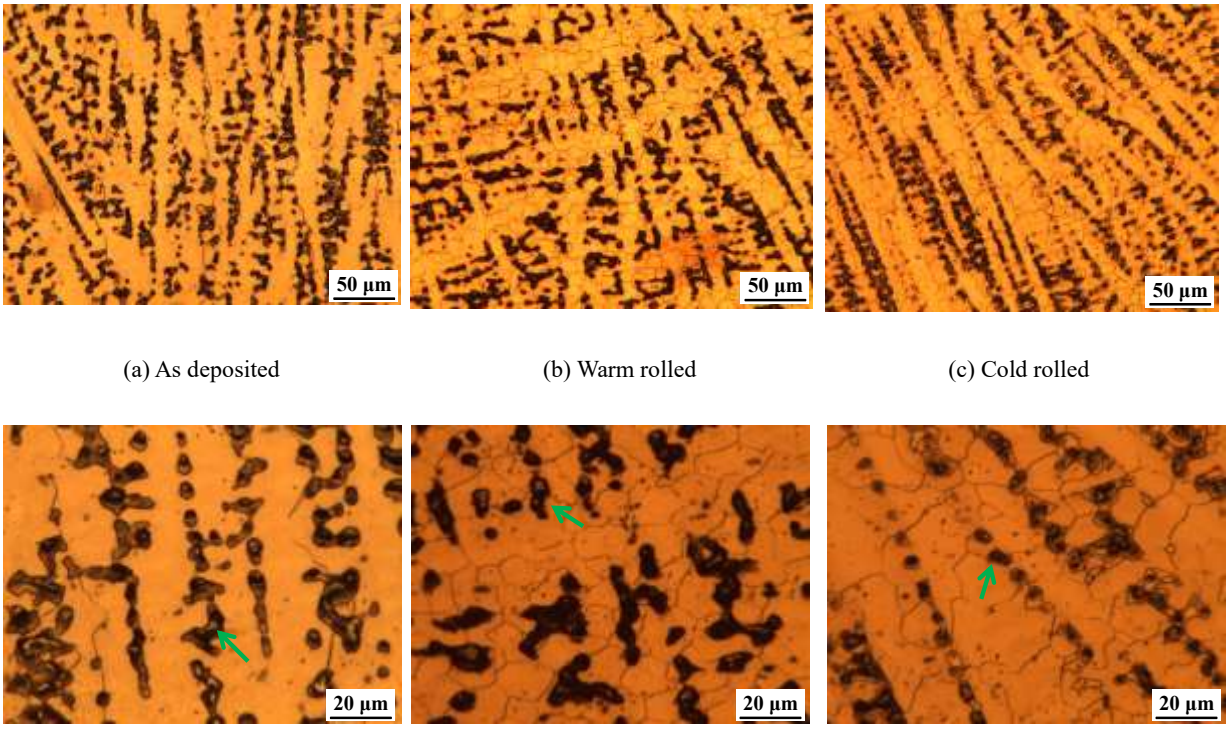

(a) As deposited (b) Warm rolled (c) Cold rolled

(d) As deposited (e) Warm rolled (f) Cold rolled

Fig.8 Microstructure of IN-718 before heat treatment: (a)-(c) with low magnification; (d)-(e) with high magnification

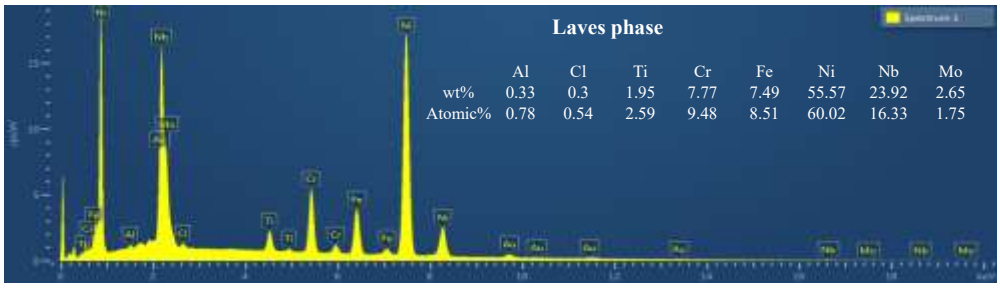

(a) Laves phase

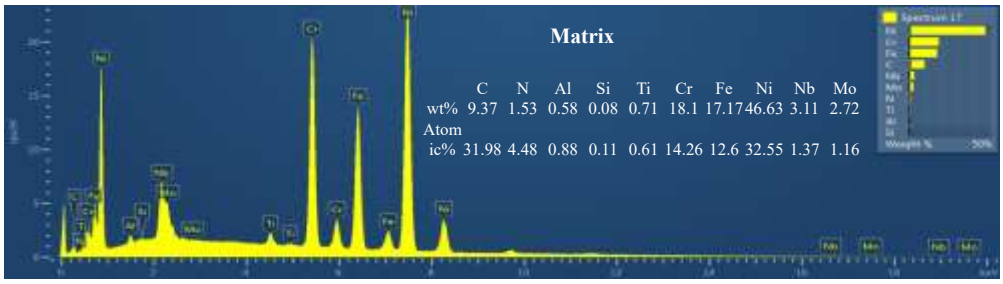

(b) Matrix of IN-718

Fig.9 Energy dispersive spectrometry (EDS) analysis precipitates during WAAM process: (a) Laves phase; (b) Matrix

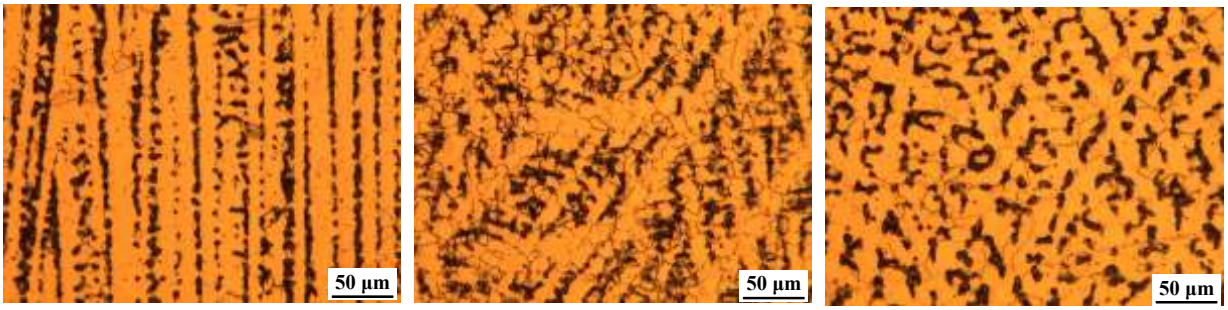

(a) As deposited (b) Warm rolled (c) Cold rolled

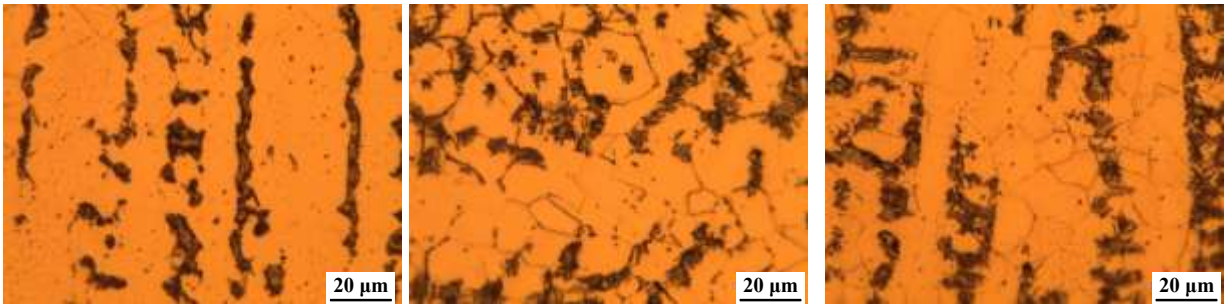

(d) As deposited (e) Warm rolled (f) Cold rolled

Fig.10 Microstructure of IN-718 after homogenization plus solution and double-aging heat treatment:

(a)-(c) with low magnification; (d)-(e) with high magnification

3.3 Precipitated phases

As shown in Fig. 11(a), discrete islands of Laves phase and some white circular MC carbides are formed at the inter-dendritic boundaries. The main composition of MC is TiN and NbC, according to the EDS analysis in Fig. 12(a). The grain boundary (GB) has a characteristic of rolled material, which can be seen from the distribution of the Laves phase in Fig. 10(b) and (c), and it is quite different to the columnar pattern of the distribution of Laves phase in as-deposited sample. A large amount of acicular δ phase appears at the grain boundary and also clusters around Laves phase for both rolled conditions. The rolling process may have influence in breaking the Laves phase and MC particles into small pieces. However, they exist in rolled material as rolling cannot completely eliminate these particles. There is some small white circular phase precipitated inside the grain for the cold rolled material, which is proved as the strengthening γ" phase based on the EDS result in Fig. 12(c). The main elements for the acicular δ phase and the circular γ" phase are Ni and Nb. Zhang et al. (2015) analyzed the atomic fraction of Nb in different phases, concluding that the atomic fraction of Nb was about 6-8% for the δ phase, 4% for the γ" phase and 10-12% for the Laves phase. In fact, there is another strengthening γ' phase for IN-718 after heat treatment, which Nb atomic fraction is less than 4%. However, it is not possible to see it clearly under SEM as its size is only a few nanometers and its volume fraction is much smaller than that of the γ" phase. Different to the cold rolling, there is much more strengthening γ" phase in the warm rolled sample which consists of the grain boundary precipitated γ" and intra-granular γ" phase, as show in Fig. 11(d) with higher magnification. Meanwhile, it can be seen that acicular δ phase is generated on GB. The larger amount of strengthening phase with dispersive distribution in the warm rolled sample results in higher strength compared to the cold rolled material.

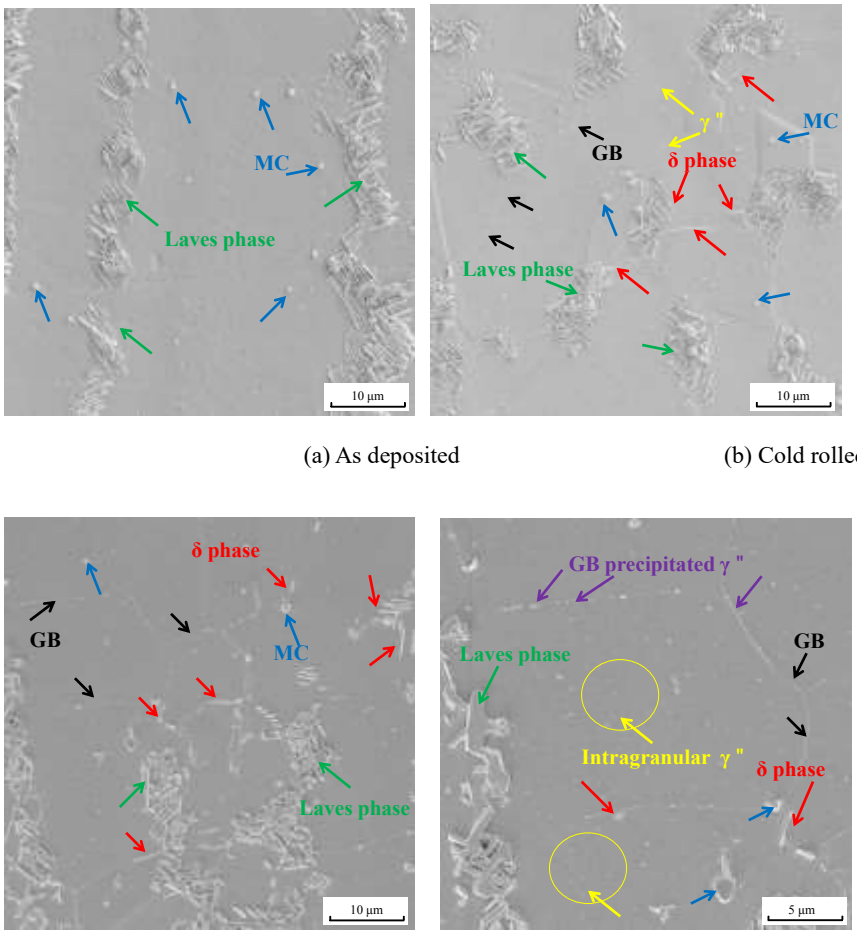

(a) As deposited (b) Cold rolled

(c) Warm rolled (d) High magnification of warm rolled

Fig.11 Precipitation phases in IN-718 after HSA heat treatment (a)WAAM deposited; (b)cold rolled; (c) warm rolled with low magnification; (d) warm rolled with low magnification (Arrows with different color refer to different precipitates)

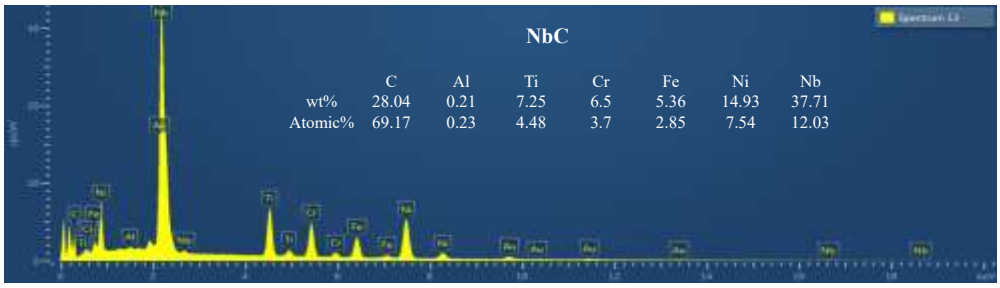

(a) NbC carbide

(b) δ phase

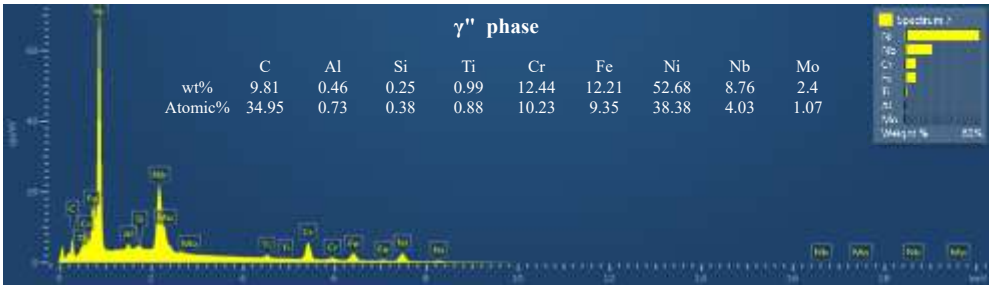

(c) γ" phase

Fig.12 Energy dispersive spectrometry (EDS) analysis results of different precipitates after HSA treatment: (a) NbC carbide; (b) δ phase; (c) γ" phase

3.4 Tensile properties

Fig.13 shows the stress-strain curves of as deposited, cold and warm rolled IN-718 before heat treatment at both horizontal and vertical directions. It can be seen that cold rolling increase the strength and reduce the elongation from Fig.14. This suggests that the work hardening induced from the rolling process increases the dislocation density inside the material thereby enhancing the strength. The increase in strength and reduction in elongation is less for the warm rolling compared to the cold rolling without heat treatment. The resistance of the material decreases with increased temperature, and the dislocation density inside the material will significantly decrease under higher temperature through the dislocation climbing and sliding. There are work hardening and dynamic recovery for the warm rolling, while there is only work hardening for the cold rolling. The strengths of the material are related to the dislocation density, as a result, the dislocation decrease in the warm rolling leads to

the decrease of UTS and YS of warm rolled samples. In order to quantitatively investigate the extent of work hardening induced by the cold and warm rolling, Hollomon equation is adopted, as shown in Eq.(2). The coefficient and exponent of strain hardening can be obtained through the stress-strain curves, as shown in Table 4. The rolling process significantly increases the strain hardening exponent at both directions. The strain hardening exponent in warm rolling is smaller than that in cold rolling process, which is consistent with the discussion above. It should be noted that the error bar for warm rolling is larger due to the non-uniform rolling temperature using flame heating, which is consistent with the microhardness results. The difference of strain hardening exponent between horizontal and vertical direction is smaller in warm rolling compared to that in cold rolling, thus resulting in more uniform strengths and elongation of the warm rolled samples.

$$\sigma=A\varepsilon^{B} \quad (2)$$

where σ is true stress, ε is true strain, A is strain hardening coefficient, B is strain hardening exponent.

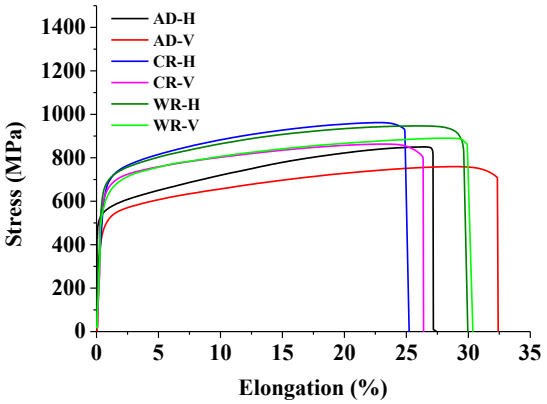

Fig.13 Stress-strain curves during tensile test under different conditions (H: horizontal; V: vertical)

Table 4 Strain hardending parameters under different conditions

Parameters	AD-H	AD-V	CR-H	CR-V	WR-H	WR-V
A	518.5	531.2	574.7	553.1	543.7	550.8
B	0.150	0.141	0.171	0.162	0.159	0.154

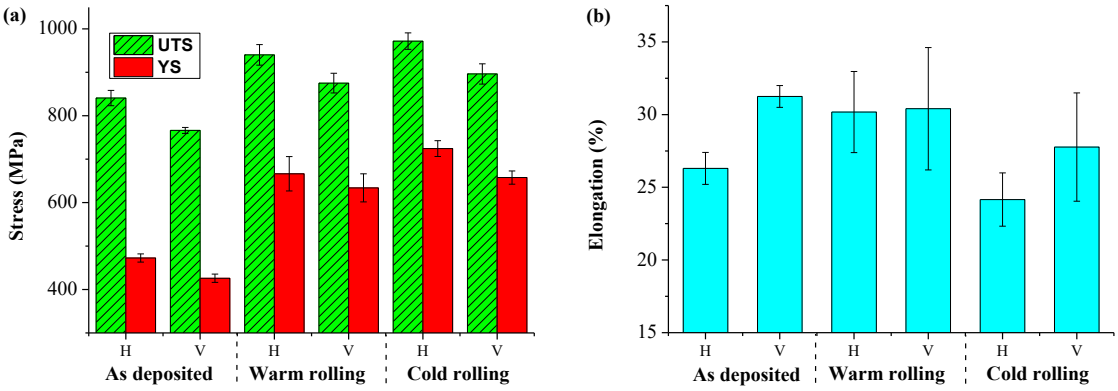

Fig.14 Tensile test results of IN718 before heat treatment: (a) UTS and YS; (b) elongation (H: horizontal; V: vertical)

Although larger deformation is generated during the warm rolling, the hardness after the warm rolling is slightly lower than that in the cold rolling. It is known that deformation resistance decreases with increased temperature. There is significant anisotropy for all samples. To quantitatively describe the anisotropy we can define an anisotropy coefficient, as shown in Eq.(3).

$$\alpha=(V_1-V_2)/V_1*100\% \quad (3)$$

where α is the anisotropy coefficient, V_1 is the larger value for specified parameter at two directions during tensile test and V_2 is the smaller one.

As shown in Fig 8 (a), columnar dendrites are the typical microstructure in WAAM deposited IN-718, the size of the dendrite in vertical direction can be several millimeters and is much larger than that in horizontal direction. According to Hall-Petch relationship, the metal yield strength is inversely proportional to the square root of the grain size.

Defects such as microvoids and secondary cracks usually appear at grain boundaries of the material during tensile test, providing paths for crack propagation resulting in reduced elongation. The anisotropy of elongation for horizontal and vertical tensile coupons can be explained in Fig.15. The defects formed at grain boundaries will be extended and coalesce in horizontal tensile coupon when applying a horizontal tensile load, which may

expedite fracture and reduce the elongation during a tensile test. However, grain boundaries will not be a path for crack propagation if the tensile force is applied in vertical direction of the vertical tensile coupon, which results in larger elongation.

Compared to the as-deposited and cold rolled samples, warm rolling significantly reduces the amount of anisotropy, as shown in Fig.16. The finer equiaxed grains and more uniform grains distribution contribute to isotropy improvement of tensile properties.

Table 5 shows tensile test results of IN-718 after SA and HSA heat treatment. In all cases there is a significant increase in both strength but reduction in elongation for all heat treatments. The precipitation of the strengthening phases, such as γ' and γ", contribute to strength improvement after heat treatments. However, the precipitated phases will impede the dislocation movement inside the material, which decreases the elongation. Nevertheless, the strength of as deposited material after heat treatment is still lower than the wrought material (Wrought AMS5662). It should be noted that the elongation for the as deposited material, before or after heat treatments is larger than that in wrought state. There are slight increases of strengths and elongation for all samples after HSA treatment compared to that in standard SA treatment.

Fig.17 shows anisotropy coefficient variation during tensile test after standard SA and HSA heat treatments. It shows that the anisotropy coefficient decreases after the SA treatment compared to the results in Fig.16, especially for the anisotropy of elongation. The anisotropy of the mechanical properties can be further decreased after HSA heat treatment and the warm rolled material shows the most isotropic properties.

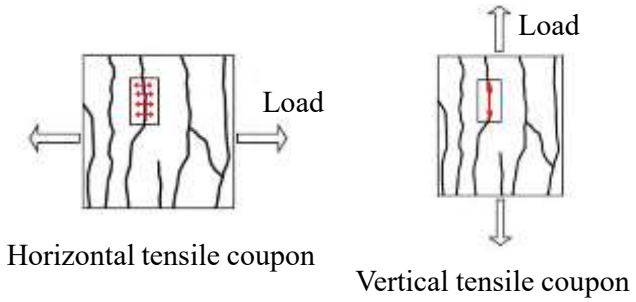

Fig.15 Schematic diagram of different fracture mode: (a) Horizontal tensile coupon; (b) Vertical tensile coupon.

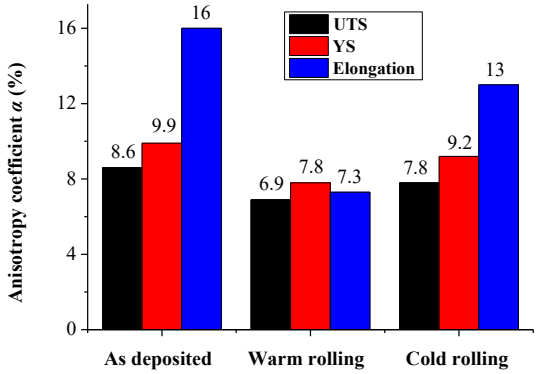

Fig.16 Anisotropy variation before heat treatment

Table 5 Tensile test results of IN718 after SA and HSA heat treatments

	UTS/MPa		YS/MPa		Elongation (%)	
	H	V	H	V	H	V
AD-SA	1158±18.2	1217.3±31	836.3±18.8	771.9±30.9	16.44±1.24	19.92±2.89
AD-HSA	1175.4±12.4	1234.6±7.4	946.5±38.5	1008.3±10.4	18.8±0.3	20.17±2.04
WR-SA	1341.5±20.5	1282.5±20.5	1085.5±23.3	1011±22.6	15.7±1.13	16.95±1.2
WR-HSA	1345±33.94	1350±23.76	1122±25.46	1098±31.11	18.6±0.28	19.15±0.78
CR-SA	1330.4±4.3	1264.4±2.9	1035±9.9	960.5±27.7	13.75±1.5	15.59±0.35
CR-HSA	1339.85±22.84	1285.8±18.1	1092.5±20.51	1065.75±19.45	16.1±0.57	17.1±0.99

Wrought AMS5662 (S.A.E 2009)	1276	1034	12

H: horizontal; V: vertical

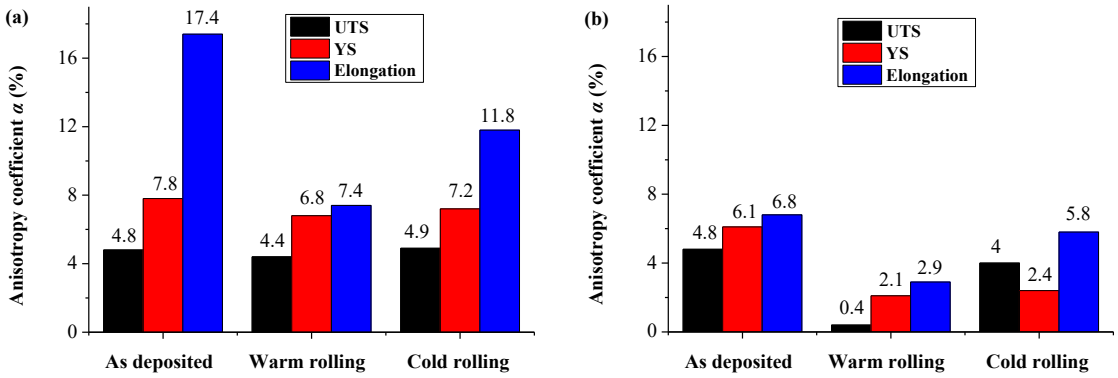

Fig.17 Anisotropy variation during tensile test after (a) standard SA and (b) HSA heat treatment

3.5 Fracture morphology

The fracture surfaces of the tensile samples before heat treatment are examined with SEM, as shown in Fig. 18. Similar to the dendritic microstructure for the as deposited samples, columnar dendritic pattern with fine dimples are exhibited, which indicates that trans-granular ductile fracture mode is generated for the as deposited samples and it results in a good elongation. Therefore, the ductile fracture is mainly generated along the inter-dendritic grain area. For the rolled surfaces, uniformly distributed dimples are generated, which is similar to the microstructure for the rolled material shown in Fig.8. The dimples in the rolled material are quite shallow and it can be seen that some particles (shown with yellow arrow) are precipitated inside the dimples and on the fracture surface. According to the EDS analysis, these particles are proved to be brittle Laves phase and MC carbides. These particles provide positions for microvoid formation and cause trans-granular ductile fracture through microvoid coalescence and propagation during tensile tests. More precipitated brittle particles and shallower dimples contribute to smaller elongation in the rolled samples compared to the as deposited ones.

After HSA heat treatment, the columnar dendritic pattern changes to fine shallow dimples for the as deposited

material, which results in a 8%~10% reduction of elongation compared to that without heat treatment, as shown in Fig.19. The fracture surfaces of rolled materials consist of shallower dimples and a few islands of flat area. The grains are significantly coarsened after heat treatment, as shown in Fig.10. The flat grain boundary area and the coarsened grains will induce crack initiation and propagation, which will decrease the elongation.

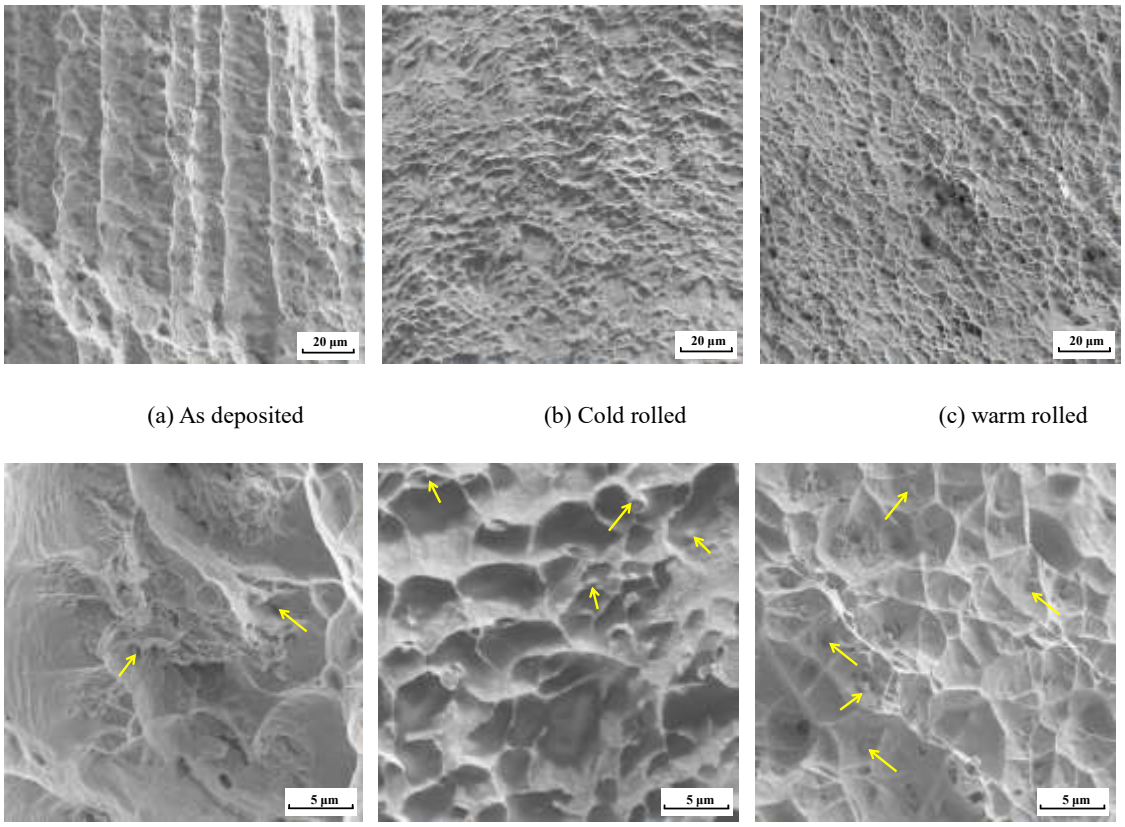

(a) As deposited (b) Cold rolled (c) warm rolled

(d) As deposited (e) Cold rolled (f) warm rolled

Fig.18 Fracture surfaces of tensile test before heat treatment: (a)-(c) at low magnification; (d)-(f) at high magnification

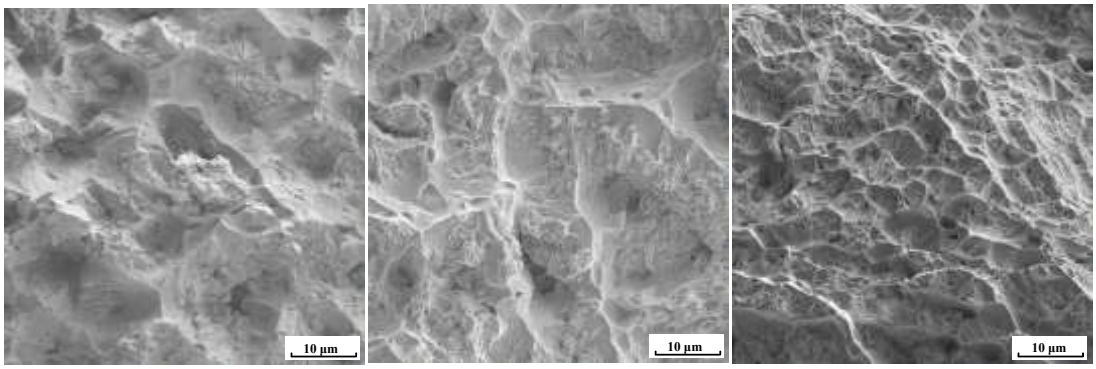

(a) As deposited (b) Cold rolled (c) Warm rolled

Fig.19 Fracture surfaces of tensile test after HSA heat treatment: (a) as deposited; (b) cold rolled; (c) warm rolled

3.6 Strengthening mechanism

Based on above analysis, the columnar microstructure for WAAM deposited material leads to inferior strengthening effect and anisotropy of mechanical properties. The work hardening process and the change of columnar dendrites to equiaxed grains in rolling processes are beneficial for strengths increase and reduction of anisotropy of mechanical properties. The precipitation of strengthening phases in both heat treatments contributes significantly to the increases of strengths.

Columnar dendrite is inevitably generated during WAAM deposition of IN 718 due to its high thermal input and directional thermal cycle. The columnar microstructure causes inferior strengthening effect and anisotropy of mechanical properties on the basis of Hall-Petch relationship. The fragmentation of large columnar dendrites and work hardening effect results from rolling process contribute to strength increase. The warm rolled samples show lower microhardness and strengths before heat treatment compared to the cold rolled condition, which is reversed after heat treatment. This can be explained as follows: both the rolling process increase the dislocation density inside the material; while some part of the accumulated dislocation density will be recovered at higher temperature in warm rolling compared to that in cold rolling. As discussed in Section 3.3, both rolling processes significantly increase the exponent of strain hardening, meanwhile, the exponent of strain hardening in cold rolling is larger than that in warm rolling process. Therefore, the work hardening effect in the cold rolling is stronger than that in warm rolling, thus resulting in higher microhardness and strengths before heat treatment. Nevertheless, the precipitation of strengthening phases is the main reason for the strength enhancement after heat treatment. The grain size in warm rolling is smaller than that in cold rolling. The uniformly distributed finer grains in warm rolling provide more grain boundaries for precipitation of strengthening phases compared to that in cold

rolling, as shown in Fig.11. Therefore, the large amount of strengthening with dispersive distribution leads to higher micohardness and strengths in warm rolling after heat treatment. However, the grain boundary and precipitated particles will impede the dislocation movement and cause the reduced elongation of the material. In addition, the Laves phase can MC carbides may become the sites for fracture initiation as they are relatively weak sites compared to the γ' and γ" strengthening phases.

For HSA heat treatment, as the homogenization temperature exceeds the dissolving temperature of the δ phase, some portion of the δ phase is partially dissolved into the matrix, as shown in Fig.10. The atomic fraction of Nb in the δ phase is 6~8% and the Nb distribution is relatively uniform due to the intense atom diffusion at the high temperature. As a result, the dissolved Nb contributes to the precipitation of the strengthening γ' and γ" phase. It is known that Nb is an important element for precipitation strengthening of IN-718 and a large amount of Laves phase and the δ phase deplete the Nb fraction of the matrix. Although HSA heat treatment causes grain growth, it has dissolved a number of the δ phase and released a portion of Nb into the material, which is essential for the subsequent precipitation of the strengthening phases. In addition, the acicular δ phase precipitates at the grain boundary and the grain interior become the obstacle for grain migration. As a result, the tensile strength is further increased with HSA compared to the standard SA heat treatment.

The reduction of elongation in both rolling processes can be summarized as follows: first, the dislocation density is increased in rolling processes and the high entangled dislocation density will impede the grain boundary motion. In addition, the precipitated strengthening phases cause dislocation pinning and hinder the dislocation movement. The brittle Laves phase and MC carbides, which cannot be completely dissolved after rolling process and HSA heat treatment, provide the sites for defects initiation and crack expansion. Finally, as the acicular δ phase is incoherent with the matrix and dislocation motion cannot be consistently generated and it may be broken down at δ phase. As a result, crack initiation and microvoid coalescence will be induced on these positions and

cause a premature failure. Nevertheless, the δ phase is beneficial for toughness increase, grain refinement and improvement of mechanical strength. Therefore, appropriate δ phase is beneficial for excellent comprehensive performances of IN-718 through rational control of process parameters and heat treatment procedures.

4 Conclusions

Warm rolling using flame heating was integrated into the WAAM deposition and its effect on the microstructure and tensile properties was investigated compared to that in cold rolled and as-deposited samples. Meanwhile, two different heat treatment procedures were studied. The strengthening mechanism of the hybrid rolling process was discussed

1. The warm rolled IN 718 show superior mechanical properties after HSA treatment compared to the wrought material.

2. The columnar dendrites in as deposited sample change to finer equiaxed grains of 16.4 μm for warm rolled alloy due to the rolling induced grain refinement.

3. Isotropic mechanical properties can be obtained in warm rolled alloy due to its finer grains and uniformly distributed strengthening phases. HSA heat treatment contributes to further decrease of anisotropy coefficient.

4. Some δ phase can be dissolved into the matrix during the homogenization process, which releases more Nb for the following precipitation of γ' and γ" strengthening phases and then increase the strength.

5. Trans-granular ductile fracture mode is generated for WAAM deposited and rolled alloy. The reduced elongation is mainly caused by work hardening, grain boundary strengthening, precipitated phases and the acicular δ phase.

6. Compared to cold rolling, warm rolling can be done with a much smaller applied load and in process with the deposition. This study provides guidance for a hybrid technology to improve the microstructure uniformity and isotropy of mechanical properties for deposited IN-718. Hot forming process can be further investigated to improve the uniformity of the

microstructure and tensile properties of deposited IN-718, and the mechanism of dynamic recrystallization in hot forming process needs to be revealed.

CRediT authorship contribution statement

Tao Zhang and Huigui Li: conceptualization, experimentation, analysis and writing. Hai Gong and Yunxin Wu: methodology and analysis. Jialuo Ding and Stewart Williams: conceptualization, resources and reviews. Chenglei Diao: experimentation assistance of warm rolling. Xiaoyong Zhang: experimentation assistance of tensile test.

Declaration of Competing Interest

The authors declare that they have no known competing financial interests or personal relationships that could have appeared to influence the work reported in this paper.

Acknowledgements

The authors wish to acknowledge the financial support from State Key Laboratory for High Performance Complex Manufacturing, Central South University (ZZYJKT2021-05), China Scholarship Council (NO. 201806835007) and the WAAMMat programme industrial partners. The authors would also like to thank Flemming Nielsen for the flame heating process. The assistance with microstructure analysis from Steve Pope and Xianwei Liu is much appreciated.

Reference

Asala, G., Khan, A. K., Andersson, J., Ojo, O. A., 2017. Microstructural analyses of ATI 718Plus® produced by wire-arc additive manufacturing process. Metall. Mater. Trans. A 48, 4211-4228.

Baufeld B., 2012. Mechanical properties of INCONEL 718 parts manufactured by shaped metal deposition (SMD). J. Mater. Eng. Perform. 21, 1416–1421.

Cao, G. H., Sun, T. Y., Wang, C. H., Li, X., Liu, M., Zhang, Z. X., 2018. Investigations of γ′, γ″ and δ precipitates in heat-treated Inconel 718 alloy fabricated by selective laser melting. Mater. Charact. 136, 398-406.

Chen, Q., Zhao, Y., Strayer, S., Zhao, Y., Aoyagi, K., Koizumi, Y., Chiba, A., Xiong, W., To, A. C., 2021. Elucidating the effect of preheating temperature on melt pool morphology variation in Inconel 718 laser powder bed fusion via simulation and experiment. Addit. Manuf. 37, 101642.

Chlebus, E., Gruber, K., Kuźnicka, B., Kurzac, J., Kurzynowski, T., 2015. Effect of heat treatment on the microstructure and mechanical properties of Inconel 718 processed by selective laser melting. Mater. Sci. Eng. A 639, 647–655.

Clark, D., Bache, M. R., Whittaker, M. T., 2008. Shaped metal deposition of a nickel alloy for aero engine applications. J. Mater. Process. Tech. 203, 439-448.

Colegrove, P. A., Donoghue, J., Martina, F., Gu, J. L., Pragnell, P. B., Hönnige, J. R., 2017. Application of bulk deformation methods for microstructural and material property improvement and residual stress and distortion control in additively manufactured components. Scripta. Mater. 135, 111-118.

Coules H E., Colegrove P., Cozzolino L., Wen S., Kelleher J., 2013. High pressure rolling of low carbon steel weld seams: Part 1 - Effects on mechanical properties and microstructure. Sci. Technol. Weld. Joi. 18(1), 76-83.

Coules H E., Colegrove P., Cozzolino L., Wen S., Kelleher J., 2013. High pressure rolling of low carbon steel weld seams: Part 2 - Roller geometry and residual stress. Sci. Technol. Weld. Joi. 18(1), 84-90.

Deng, D., Peng, R. L., Brodin, H., Moverare, J., 2018. Microstructure and mechanical properties of Inconel 718 produced by selective laser melting: Sample orientation dependence and effects of post heat treatments. Mater. Sci. Eng. A 713, 294-306.

Hu Y., Ao N., Wu S., Yu Y., Zhang H., Qian W., Guo G., Zhang M., Wang G., 2021. Influence of in situ micro-rolling on the improved strength and ductility of hybrid additively manufactured metals. Eng. Fract. Mech. 253, 107868.

Jafari D., Vaneker T., Gibson I., 2021. Wire and arc additive manufacturing: Opportunities and challenges to control the quality and accuracy of manufactured parts. Mater. Design. 202, 109471.

Li, J., Zhao, Z., Bai, P., Qu, H., Liu, B., Li, L., Wu, L., Guan, R., Liu, H., Guo, Z., 2019. Microstructural evolution and mechanical properties of IN718 alloy fabricated by selective laser melting following different heat treatments. J. Alloy. Comp. 772, 861-870.

Martina, F., Colegrove, P. A., Williams, S. W., Meyer, J., 2015. Microstructure of interpass rolled wire + arc additive manufacturing Ti-6Al-4V components. Metall. Mater. Trans. A 46, 6103-6118.

Mei, Y., Liu, Y., Liu, C., Li, C., Yu, L., Guo, Q., Li, H., 2015. Effects of cold rolling on the precipitation kinetics and the morphology evolution of intermediate phases in Inconel 718 alloy. J. Alloy. Comp. 649, 949-960.

Raut L. P., Taiwade R. V., 2021. Wire arc additive manufacturing: A comprehensive review and research directions. J. Mater. Eng. Perform. 30, 4768–4791.

S.A.E. Aerospace, 2009. Aerospace Material Specification: AMS 5662, SAE International.

Schneider, J., Lund, B., Fullen, M., 2018. Effect of heat treatment variations on the mechanical properties of Inconel 718 selective laser melted specimens. Addit. Manuf. 21, 248-254.

Tucho, W. M., Cuvillier, P., Sjolyst-Kverneland, A., Hansen, V., 2017. Microstructure and hardness studies of Inconel 718 manufactured by selective laser melting before and after solution heat treatment. Mater. Sci. Eng. A 689, 220-232.

Xu, X., Ding, J., Ganguly, S., Williams, S., 2019. Investigation of process factors affecting mechanical properties of INCONEL 718 superalloy in wire+ arc additive manufacture process. J. Mater. Process. Tech. 265, 201-209.

Xu, X., Ganguly, S., Ding, J., Seow, C., Williams, S., 2018. Enhancing mechanical properties of wire+ arc additively manufactured INCONEL 718 superalloy through in-process thermomechanical processing. Mater. Design. 160, 1042-1051.

Watring, D. S., Benzing, J. T., Hrabe, N., Spear, A. D., 2020. Effects of laser-energy density and build orientation on the structure–property relationships in as-built Inconel 718 manufactured by laser powder bed fusion. Addit. Manuf. 36, 101425.

Zhang, D., Niu, W., Cao, X., Liu, Z., 2015. Effect of standard heat treatment on the microstructure and mechanical properties of selective laser melting manufactured Inconel 718 superalloy. Mater. Sci. Eng. A 644,) 32-40.

Zhang, D., Feng, Z., Wang, C., Wang, W., Liu, Z., Niu, W., 2018. Comparison of microstructures and mechanical properties of Inconel 718 alloy processed by selective laser melting and casting. Mater. Sci. Eng. A 724, 357-367.

Zhang, J., Guo, Q., Liu, Y., Li, C., Yu, L., Li, H., 2016. Effect of cold rolling and first precipitates on the coarsening behavior of γ ″-phases in

Inconel 718 alloy. Int. J. Min. Met. Mater. 23, 1087-1096.

Fig.1 Experimental set up of hybrid WAAM deposition and rolling system

Fig.2 (a): Experimental set up of flame heating; (b) Positions of thermocouples

Fig.3 Schematic diagrams of different heat treatments: (a) solution and double-aging SA; (b) homogenization plus solution and double-aging (HSA). (WQ: water quenching; FC: furnace cooling; AC: air cooling)

Fig.4 Dimensions of IN 718 tensile coupon (unit: mm)

Fig.5 Temperature variation during flame heating

Fig.6 Dimensions of three walls on different conditions: (a) wall size; (b) cross section of walls

Fig.7 Microhardness distribution of walls after deposition, cold and warm rolling process

Fig.8 Microstructure of IN-718 before heat treatment: (a)-(c) with low magnification; (d)-(e) with high magnification

Fig.9 Energy dispersive spectrometry (EDS) analysis precipitates during WAAM process: (a) Laves phase; (b) Matrix

Fig.10 Microstructure of IN-718 after homogenization plus solution and double-aging heat treatment:

(a)-(c) with low magnification; (d)-(e) with high magnification

Fig.11 Precipitation phases in IN-718 after HSA heat treatment (a)WAAM deposited; (b)cold rolled; (c) warm rolled with low magnification; (d) warm rolled with low magnification (Arrows with different color refer to different precipitates)

Fig.12 Energy dispersive spectrometry (EDS) analysis results of different precipitates after HSA treatment: (a) NbC carbide; (b) δ phase; (c) γ" phase

Fig.13 Stress-strain curves during tensile test under different conditions (H: horizontal; V: vertical)

Fig.14 Tensile test results of IN718 before heat treatment: (a) UTS and YS; (b) elongation (H: horizontal; V: vertical)

Fig.15 Schematic diagram of different fracture mode: (a) Horizontal tensile coupon; (b) Vertical tensile coupon.

Fig.16 Anisotropy variation before heat treatment

Fig.17 Anisotropy variation during tensile test after (a) standard SA and (b) HSA heat treatment

Fig.18 Fracture surfaces of tensile test before heat treatment: (a)-(c) at low magnification; (d)-(f) at high magnification

Fig.19 Fracture surfaces of tensile test after HSA heat treatment: (a) as deposited; (b) cold rolled; (c) warm rolled

Table 1 Experimental parameters for hybrid deposition and rolling process

Table 2 Size and strain of walls

Table 3 Average microhardness after heat treatments

Table 4 Strain hardending parameters under different conditions

Table 5 Tensile test results of IN718 after SA and HSA heat treatments

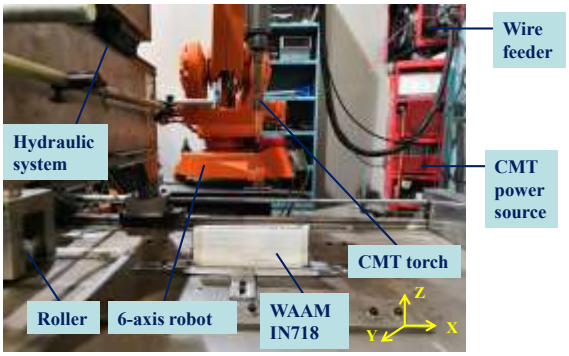

Fig.1 Experimental set up of hybrid WAAM deposition and rolling system

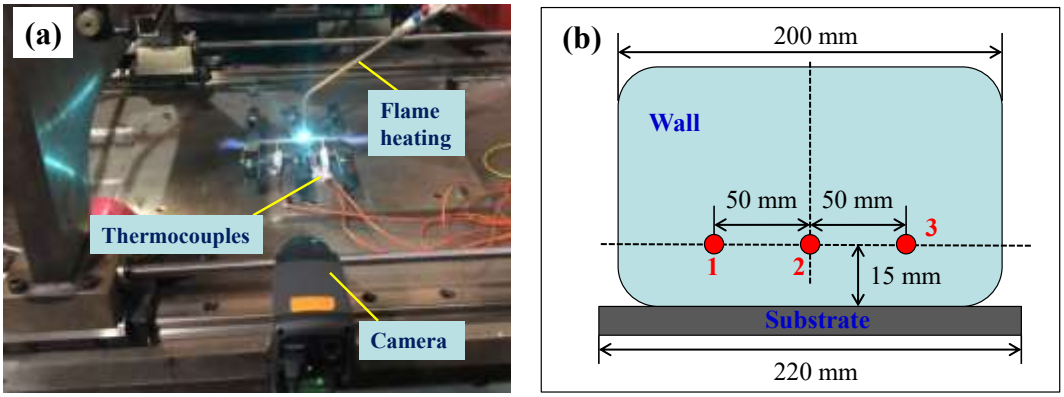

Fig.2 (a): Experimental set up of flame heating; (b) Positions of thermocouples

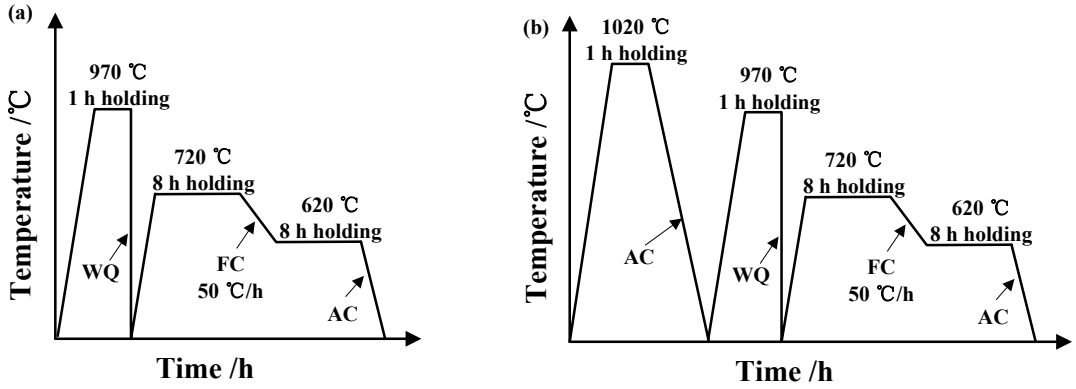

Fig.3 Schematic diagrams of different heat treatments: (a) solution and double-aging SA; (b) homogenization plus solution and double-aging (HSA). (WQ: water quenching; FC: furnace cooling; AC: air cooling)

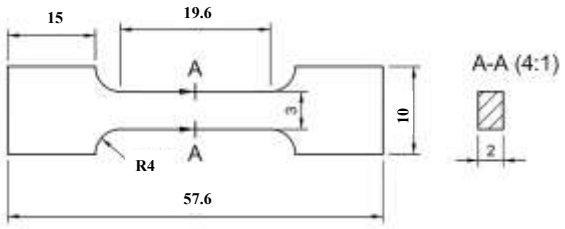

Fig.4 Dimensions of IN 718 tensile coupon (unit: mm)

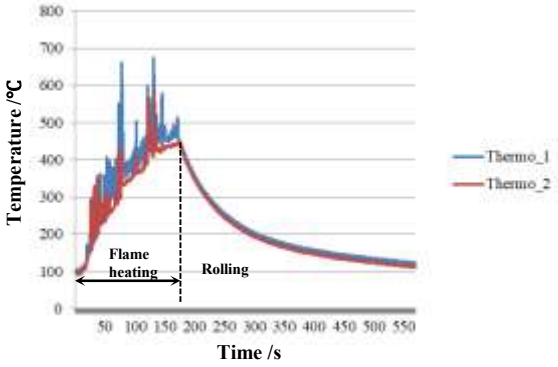

Fig.5 Temperature variation during flame heating

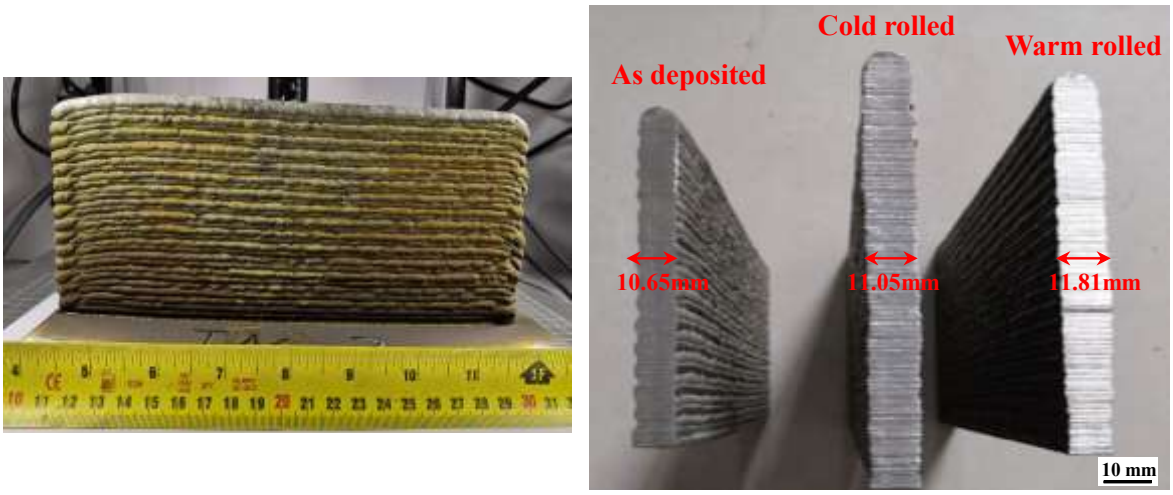

(a) Wall size (b) Cross section of walls

Fig.6 Dimensions of three walls on different conditions: (a) wall size; (b) cross section of walls

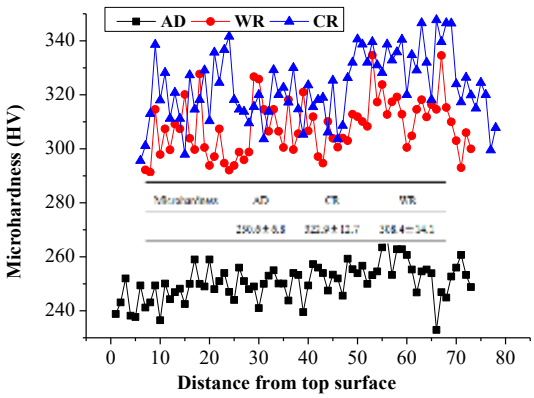

Fig.7 Microhardness distribution of walls after deposition, cold and warm rolling process

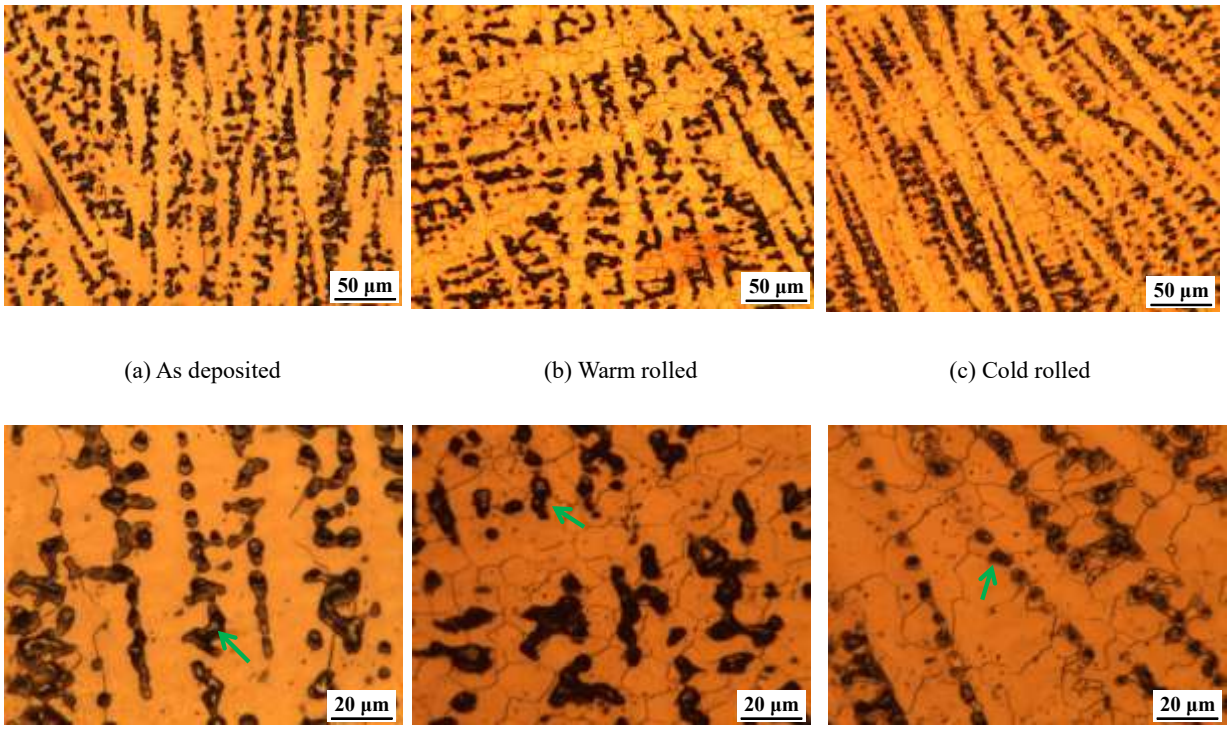

(a) As deposited (b) Warm rolled (c) Cold rolled

(d) As deposited (e) Warm rolled (f) Cold rolled

Fig.8 Microstructure of IN-718 before heat treatment: (a)-(c) with low magnification; (d)-(e) with high magnification

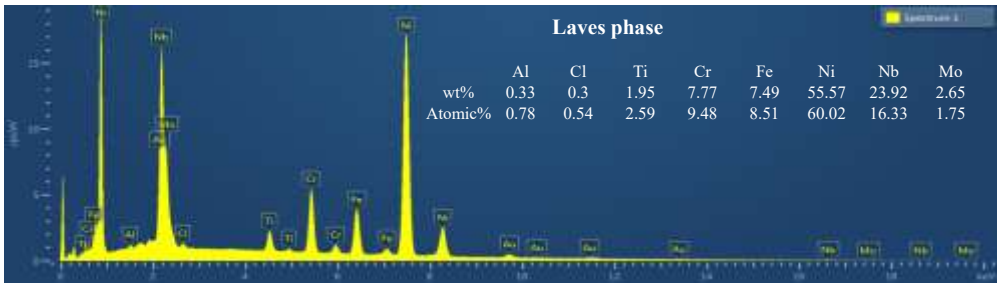

(a) Laves phase

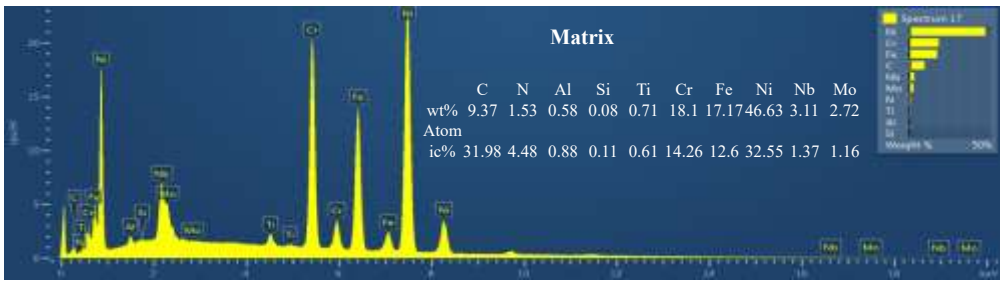

(b) Matrix of IN-718

Fig.9 Energy dispersive spectrometry (EDS) analysis precipitates during WAAM process: (a) Laves phase; (b) Matrix

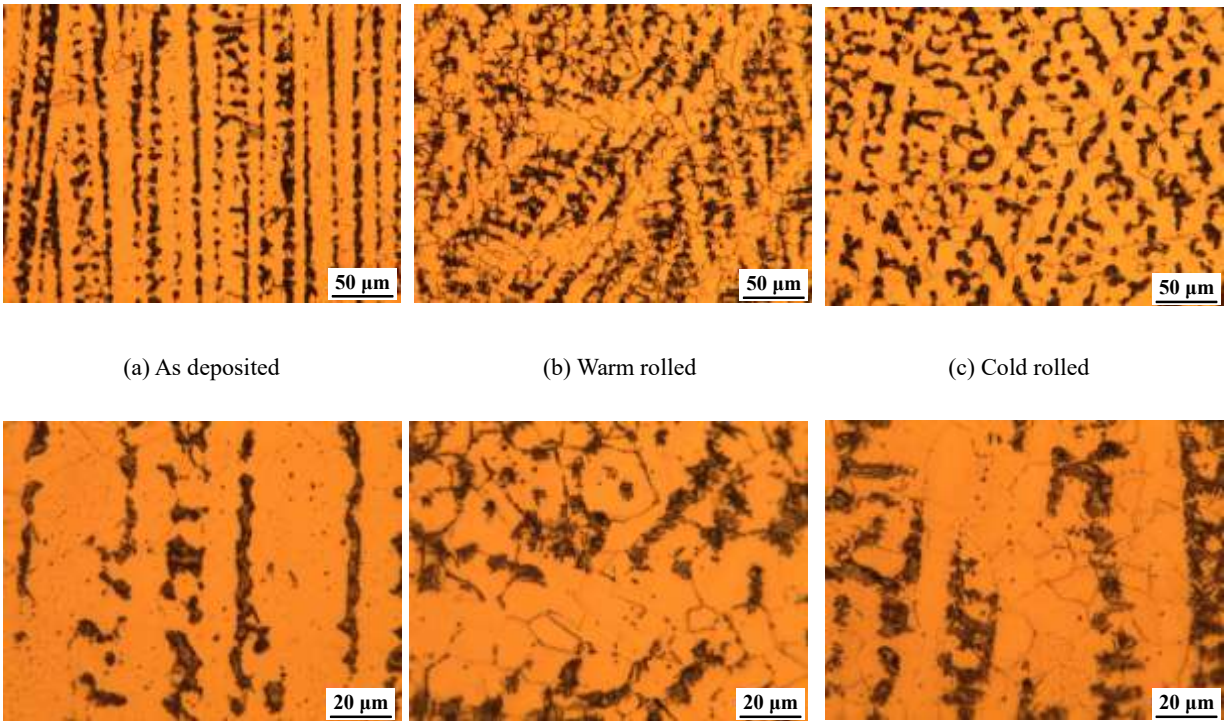

(a) As deposited (b) Warm rolled (c) Cold rolled

(d) As deposited (e) Warm rolled (f) Cold rolled

Fig.10 Microstructure of IN-718 after homogenization plus solution and double-aging heat treatment:

(a)-(c) with low magnification; (d)-(e) with high magnification

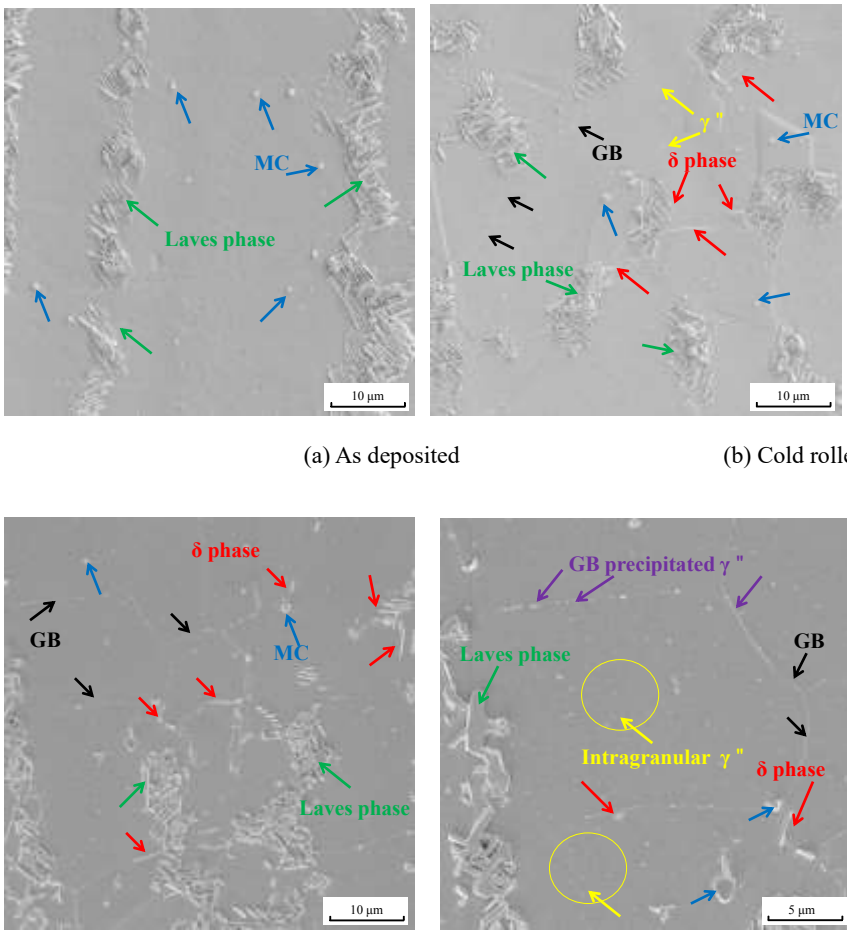

(a) As deposited (b) Cold rolled

(c) Warm rolled (d) High magnification of warm rolled

Fig.11 Precipitation phases in IN-718 after HSA heat treatment (a)WAAM deposited; (b)cold rolled; (c) warm rolled with low magnification; (d) warm rolled with low magnification (Arrows with different color refer to different precipitates)

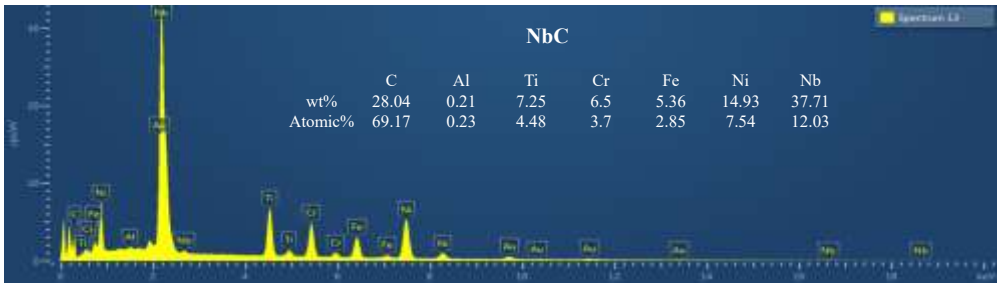

(a) NbC carbide

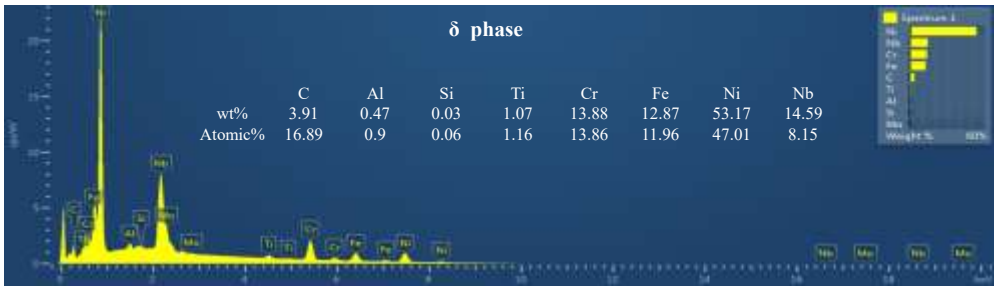

(b) δ phase

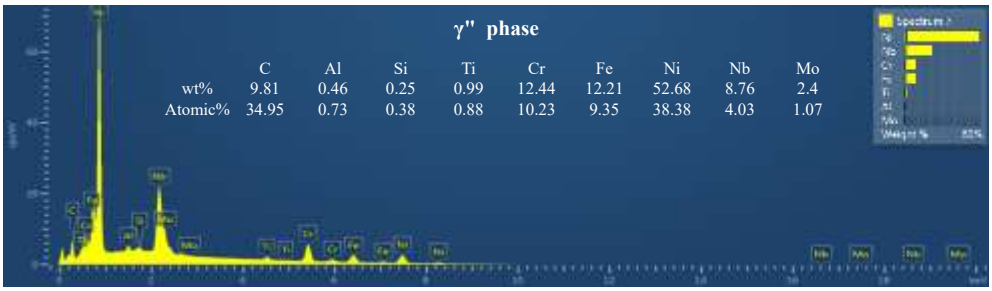

(c) γ" phase

Fig.12 Energy dispersive spectrometry (EDS) analysis results of different precipitates after HSA treatment: (a) NbC carbide;

(b) δ phase; (c) γ" phase

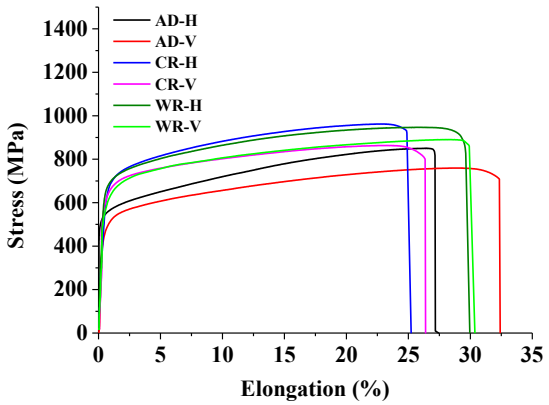

Fig.13 Stress-strain curves during tensile test under different conditions (H: horizontal; V: vertical)

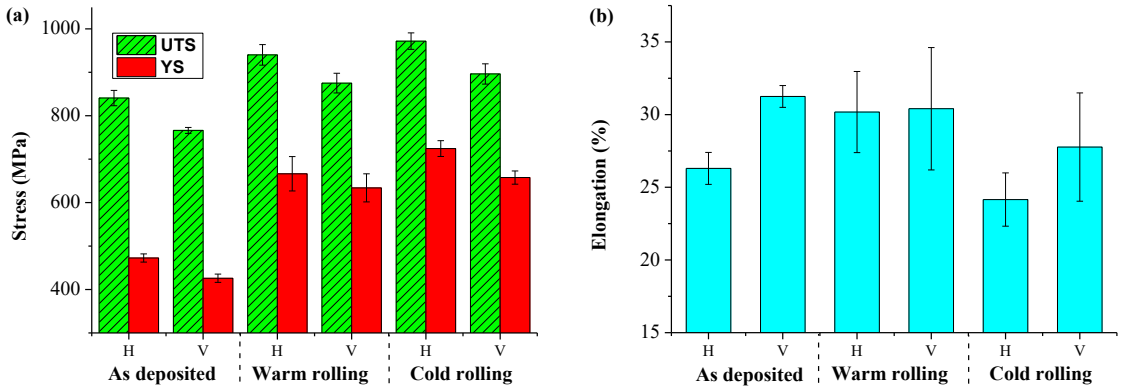

Fig.14 Tensile test results of IN718 before heat treatment: (a) UTS and YS; (b) elongation (H: horizontal; V: vertical)

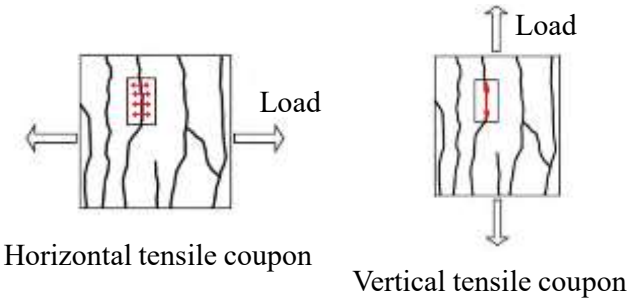

Fig.15 Schematic diagram of different fracture mode: (a) Horizontal tensile coupon; (b) Vertical tensile coupon.

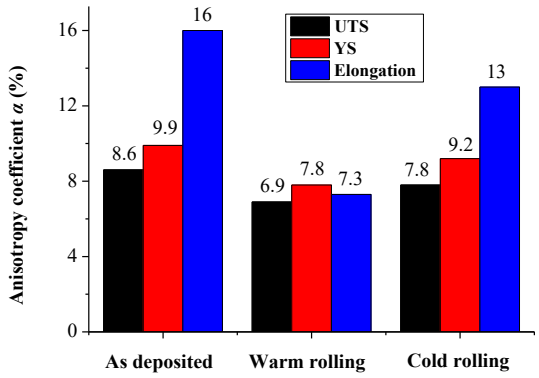

Fig.16 Anisotropy variation before heat treatment

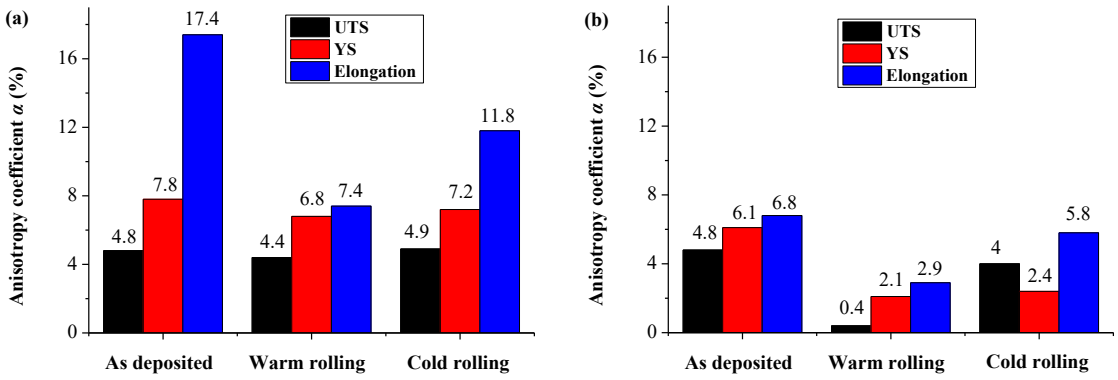

Fig.17 Anisotropy variation during tensile test after (a) standard SA and (b) HSA heat treatment

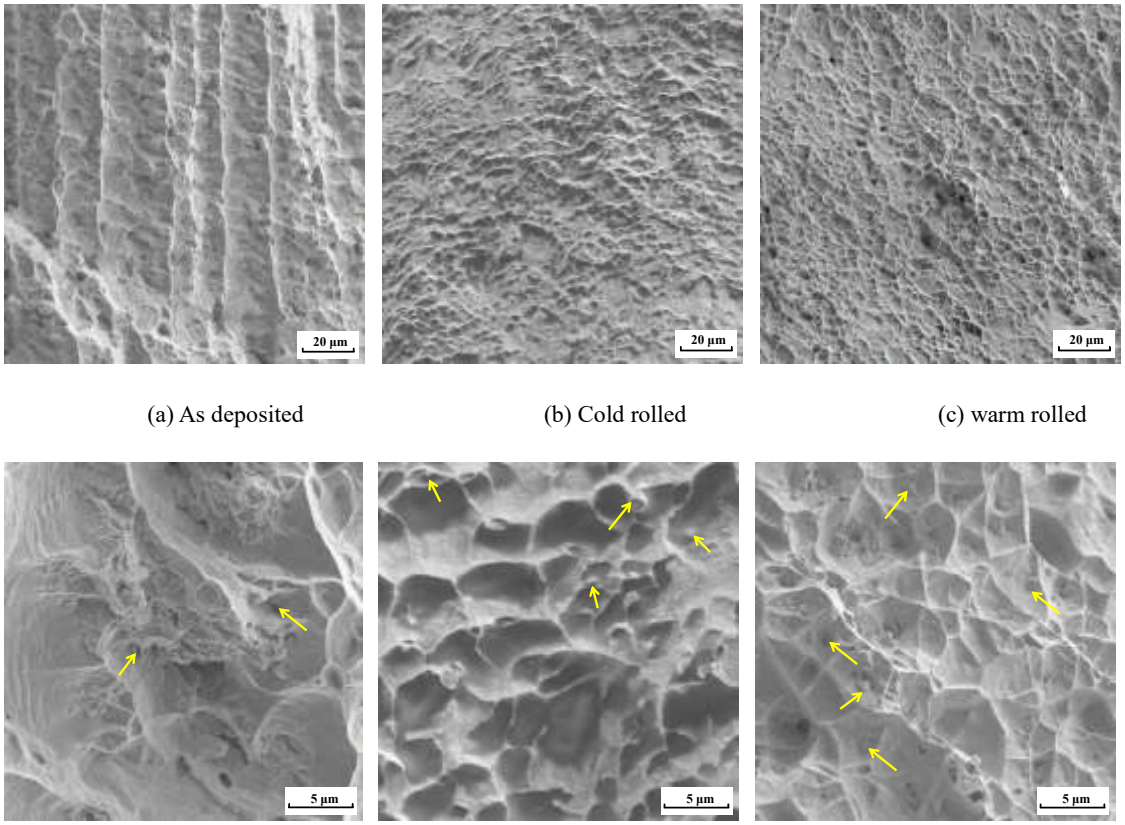

(a) As deposited (b) Cold rolled (c) warm rolled

(d) As deposited (e) Cold rolled (f) warm rolled

Fig.18 Fracture surfaces of tensile test before heat treatment: (a)-(c) at low magnification; (d)-(f) at high magnification

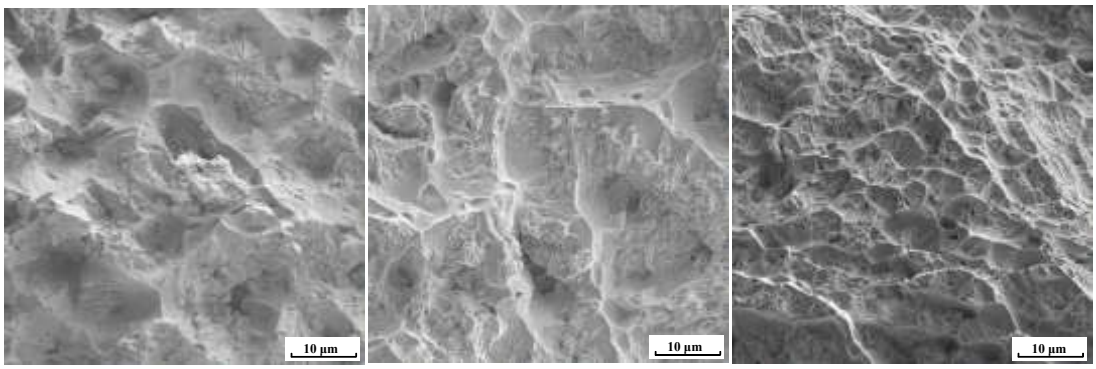

(a) As deposited (b) Cold rolled (c) Warm rolled

Fig.19 Fracture surfaces of tensile test after HSA heat treatment: (a) as deposited; (b) cold rolled; (c) warm rolled

2021-09-08

Hybrid wire - arc additive manufacture and effect of rolling process on microstructure and tensile properties of Inconel 718

Zhang, Tao

Elsevier

Zhang T, Li H, Gong H, et al., (2022) Hybrid wire - arc additive manufacture and effect of rolling process on microstructure and tensile properties of Inconel 718. Journal of Materials Processing Technology, Volume 299, January 2022, Article number 117361

10.1016/j.jmatprotec.2021.117361